

# Localization for MCMC: sampling high-dimensional posterior distributions with banded structure\*

Matthias Morzfeld<sup>†</sup>, Xin T. Tong<sup>‡</sup>, and Youssef M. Marzouk<sup>§</sup>

**Abstract.** We investigate how ideas from covariance localization in numerical weather prediction can be used to construct effective Markov chain Monte Carlo (MCMC) methods for sampling high-dimensional distributions with banded covariance and precision matrices. The main idea is to exploit banded structure during problem formulation and numerical solution. In particular, we propose to solve high-dimensional Bayesian inverse problems with nearly banded structure (i.e., small off-diagonal elements) by first replacing the problem with a banded version, and then solving the modified problem using a Metropolis-within-Gibbs sampler that exploits this banded structure. We discuss conditions under which posterior moments of the modified problem are close to those of the original problem. Under the same conditions, the convergence rate of an associated sampler is independent of dimension. We present our ideas in the context of Gaussian problems, where mathematical formulations are precise and for which convergence analysis can be made rigorous.

**Key words.** Markov chain Monte Carlo, Bayesian inverse problems, high dimensions, localization, dimension-independent convergence

**AMS subject classifications.** 65C05, 80M31, 62C10, 74G75

**1. Introduction and motivation.** Consider using a Markov chain Monte Carlo (MCMC) algorithm to sample an  $n$ -dimensional Gaussian distribution  $p(x) = \mathcal{N}(0, \mathbf{I})$ , where  $\mathbf{I}$  is the identity matrix of dimension  $n$ . Suppose that the current state of the Markov chain is  $\mathbf{x}_k$ . Then the Metropolis-Hastings (MH) algorithm proposes a move to  $\mathbf{x}'_{k+1}$  by drawing from a proposal distribution  $q(\mathbf{x}'_{k+1}|\mathbf{x}_k)$ , and accepts or rejects the move with probability

$$a_{k+1} = \max \left\{ 1, \frac{p(\mathbf{x}'_{k+1})q(\mathbf{x}_k|\mathbf{x}'_{k+1})}{p(\mathbf{x}_k)q(\mathbf{x}'_{k+1}|\mathbf{x}_k)} \right\};$$

see, e.g., [27, 31, 36]. Averages over the samples generated in this way converge to expected values with respect to the target distribution  $p$  as  $k \rightarrow \infty$ . A question of practical importance is: *how many samples are needed to accurately estimate expectations with respect to the target distribution?* The answer depends on the proposal distribution. For a Gaussian proposal

---

\*Submitted to the editors DATE.

**Funding:** M. Morzfeld gratefully acknowledges support by the Office of Naval Research (grant number N00173-17-2-C003), by the National Science Foundation (grant DMS-1619630), and by the Alfred P. Sloan Foundation (Sloan Research Fellowship). X.T. Tong gratefully acknowledges support by the National University of Singapore (grant R-146-000-226-133). Y. Marzouk gratefully acknowledges support from the DOE Office of Advanced Scientific Computing Research (grant DE-SC0009297).

<sup>†</sup>Department of Mathematics, University of Arizona, Tucson, AZ, 85721 ([mmo@math.arizona.edu](mailto:mmo@math.arizona.edu), <http://math.arizona.edu/~mmo/>).

<sup>‡</sup>Department of Mathematics, National University of Singapore, 10 Lower Kent Ridge Road, Singapore 119076 ([mattxin@nus.edu.sg](mailto:mattxin@nus.edu.sg), <http://www.math.nus.edu.sg/~mattxin/>).

<sup>§</sup>Department of Aeronautics and Astronautics, Massachusetts Institute of Technology, 77 Massachusetts Avenue, Cambridge, MA 02139 ([ymarz@mit.edu](mailto:ymarz@mit.edu), <http://uqgroup.mit.edu>)

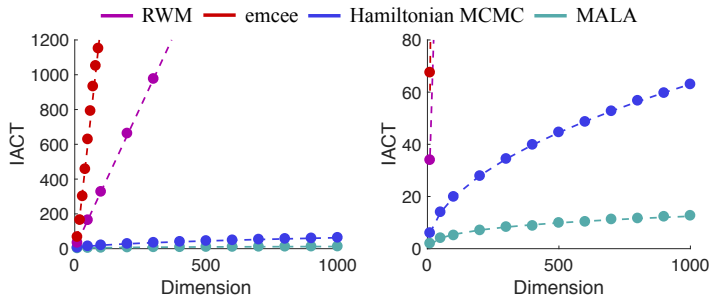


**Figure 1.1.** *IACT as a function of dimension for various MCMC methods applied to an isotropic Gaussian. Dots represent IACT, averaged over all  $n$  variables, for emcee (red), RWM (purple), Hamiltonian MCMC (blue), and MALA (teal). The dashed lines represent linear fits (emcee and RWM), fits to a square root (Hamiltonian MCMC), and a fit to a 1/3-degree polynomial (MALA).*

distribution  $q(\mathbf{x}_{k+1}|\mathbf{x}_k) = \mathcal{N}(\mathbf{x}_k, \sigma^2 \mathbf{I})$ , which produces a so-called random walk Metropolis (RWM) chain, one must choose the step-size  $\sigma$  such that the acceptance probability is reasonably large while, at the same time, the accepted MCMC moves are large enough to explore the space appropriately. An optimal choice that achieves this trade-off for RWM is  $\sigma^2 = O(n^{-1})$ , where  $n$  is the dimension of the problem; see, e.g., [4, 44, 45]. Optimal scalings of the step-size with problem dimension are also known for other MCMC algorithms. For example, the proposal distribution of the Metropolis-adjusted Langevin algorithm (MALA) is defined by

$$\mathbf{x}'_{k+1} = \mathbf{x}_k + \frac{\sigma^2}{2} \nabla \log p(\mathbf{x}_k) + \sigma \xi$$

where  $\nabla$  denotes a gradient and  $\xi$  is a vector of  $n$  standard normal variates. An optimal choice for the step-size is  $\sigma^2 = O(n^{-1/3})$ . For Hamiltonian Monte Carlo (see, e.g., [15, 35]) an optimal step-size is  $O(n^{-1/4})$  [3].

Setting aside issues of transient behavior [10], the efficiency of an MCMC algorithm can be assessed by computing the integrated auto-correlation time (IACT). Throughout this paper we use the definitions and numerical approximations of IACT discussed in [55]. Heuristically, the number of effective samples is the number of samples divided by IACT; see, e.g., [27, 31]. In Figure 1.1 we compute IACT for various MCMC algorithms applied to the  $n$ -dimensional isotropic Gaussian, as a function of  $n$ . We observe that IACT grows with dimension for all algorithms we consider, but at different rates. For both RWM and an affine invariant sampler [18, 22] called emcee or MCMC Hammer, IACT grows linearly with the dimension  $n$ ; for Hamiltonian MCMC, we observe that IACT grows with the square root of  $n$ , while for MALA, IACT grows as  $n^{1/4}$ .

If this cartoon example were indicative of “real-world” problems, then IACT may be in the hundreds or more for a problem with millions of variables, which makes computations expensive. The purpose of this paper is to address this issue in the context of Bayesian inverse problems. We explain that the isotropic Gaussian is a meaningful cartoon for how the performance of MCMC scales *as the size of the domain and the number of observations increase*. Such an increase can lead to high-dimensional problems that have *banded* structure, i.e., banded covariance and precision matrices. Our main message is that one can design com-

putationally efficient MCMC methods for such problems. This is a different setting than that addressed by current MCMC literature on discretization-invariant or dimension-independent algorithms, which focuses on how computational requirements scale as a grid is refined; see, e.g., [2, 8, 11–13, 17, 23, 33, 38]). Grid refinement increases the number of apparent dimensions, but keeps the size of the domain, and the number of observations, fixed.

Our ideas are inspired by covariance localization of the ensemble Kalman filter (EnKF) in numerical weather prediction (NWP) [16, 51]. Localization, which enforces and exploits the fact that covariance matrices are banded, makes it possible to estimate forecast covariances of a state vector whose dimension can exceed  $10^8$ , with sample size of less than 100. Our study presents a first step towards leveraging these ideas in Bayesian inverse problems where MCMC techniques are often used. We focus on Gaussian problems because the proofs of our theorems are more manageable in this case. Moreover, we only consider banded covariance or precision matrices, which arise, for instance, in linear–Gaussian Bayesian inverse problems on one-dimensional spatial domains (see our examples in Section 5). We anticipate that many of our ideas can be adapted to matrices with more general sparsity patterns, but defer this investigation to future work.

This paper is organized as follows. In Section 2 we consider the Gibbs sampler and show that an upper bound for its convergence rate is dimension independent for Gaussian target distributions with banded covariance matrices. We also show that an upper bound for the convergence rate is dimension independent if the precision matrix is banded. In both cases, however, the upper bound for the convergence rate depends on the condition number of the covariance or precision matrix. Convergence is fast only if the condition number is moderate. A moderate condition number in fact ties our assumptions together: a banded precision matrix implies a nearly banded covariance matrix and vice versa, when the condition number is moderate [6]. In Section 3 we describe localization of Bayesian inverse problems. We first consider localization of prior covariance matrices in Section 3.1, and show that the localized problem, which is obtained by neglecting small off-diagonal elements of the prior covariance, is a small perturbation of the unlocalized problem. We then describe a localized Metropolis-within-Gibbs (l-MwG) sampler that exploits the banded structure of the localized problem. Section 3.2 describes a precision matrix-based localization for Bayesian inverse problems and an analogous l-MwG sampler. In Section 4, we discuss the physical interpretations of our assumptions and compare them to current notions of low dimensionality in Bayesian inverse problems. We illustrate our ideas with numerical examples in Section 5, where we also compare l-MwG samplers to RWM, MALA, pCN [11], and Hamiltonian MCMC. The numerical examples indicate that the IACT of l-MwG can be independent of dimension in problems where the IACT of RWM, MALA, pCN, and Hamiltonian MCMC grows with dimension. Proofs of our theorems are given in the Appendix and supplementary materials.

**2. Gibbs sampling Gaussians with banded covariance or precision matrices.** Let the target probability density be  $p(\mathbf{x})$ , where  $\mathbf{x}$  is shorthand for the vector with  $n$  elements  $x_1, x_2, \dots, x_n$ . Set  $j = 1$ , and let  $\mathbf{x}^k$  be the current state of a Markov chain. Then a Gibbs sampler proceeds as follows:

- (i) Set  $k \rightarrow k + 1$ .
- (ii) Sample  $x_j^{k+1}$  from the conditional distribution  $p(x_j | x_1^{k+1}, \dots, x_{j-1}^{k+1}, x_{j+1}^k, \dots, x_n^k)$ .

(iii) Repeat for all  $n$  elements  $x_j$  of  $\mathbf{x}$ .

Repeating this process  $N_e$  times, one obtains samples such that averages over these samples converge to expected values with respect to the target density  $p$  as  $N_e \rightarrow \infty$ .

One can also use a blocked Gibbs sampler, in which one groups variables into blocks and samples joint distributions, defined over the blocks, conditioned on the other blocks. For simplicity, we assume that there are  $m$  blocks of the same size  $q$  so that  $n = mq$ . We divide the  $n$  elements of  $\mathbf{x}$  according to the  $m$  blocks and write  $\mathbf{x} = (\mathbf{x}_1, \dots, \mathbf{x}_m)$ , with the understanding that each  $\mathbf{x}_j$  consists of  $q$  consecutive elements in  $\mathbf{x}$ . We sample from the conditionals defined for each  $\mathbf{x}_j$ , i.e., at the  $k$ th step of the blocked Gibbs sampler, we sample the block  $\mathbf{x}_j$  using the  $q$ -dimensional conditional  $p(\mathbf{x}_j | \mathbf{x}_1^{k+1}, \dots, \mathbf{x}_{j-1}^{k+1}, \mathbf{x}_{j+1}^k, \dots, \mathbf{x}_m^k)$ . We call the resulting algorithm a ‘‘Gibbs sampler with block-size  $q$ ’’ because the ‘‘standard’’ Gibbs sampler above is a Gibbs sampler of block-size 1 in this terminology.

Note that the Gibbs sampler generates independent samples, independently of dimension, for the Gaussian of Section 1 with diagonal covariance and precision matrices. Similarly, the Gibbs sampler with block-size  $q$  generates independent samples, independently of dimension if the covariance or precision matrices are block-diagonal with block size  $q$ . Perhaps Gibbs samplers can be nearly as effective if the covariance or precision matrices are banded but not (block-) diagonal. We investigate this idea and study convergence rates of Gibbs samplers for Gaussian distributions with banded covariance or precision matrices.

**2.1. Gibbs sampling of distributions with tridiagonal covariance matrices.** We first consider the Gibbs sampler for Gaussian distributions with tridiagonal covariance matrices. Recall that a matrix  $\mathbf{C}$  is tridiagonal, if

$$(2.1) \quad [\mathbf{C}]_{i,j} = 0 \quad \text{for} \quad (i,j) \notin \{(i,i), (i,i+1), (i,i-1), i=1, \dots, n\},$$

where  $[\mathbf{C}]_{i,j}$  are the elements of the matrix  $\mathbf{C}$ . The convergence rate of the Gibbs sampler is dimension-independent for problems with tridiagonal covariance matrix, as detailed in the following theorem, whose proof is in Appendix A. Throughout this paper, we use  $\|\cdot\|$  to denote the  $l_2$  norm for a vector  $\mathbf{x}$  with elements  $x_1, \dots, x_n$ ,  $\|\mathbf{x}\| = \sqrt{\sum_{j=1}^n x_j^2}$ , as well as the  $l_2$  operator norm for a matrix  $\mathbf{A}$ ,  $\|\mathbf{A}\| = \sup_{v \in \mathbb{R}^n, \|v\|=1} \|\mathbf{A}v\|$ .

**Theorem 2.1.** *Suppose the Gibbs sampler is applied to a Gaussian target distribution  $p = \mathcal{N}(\mathbf{m}, \mathbf{C})$ , where the covariance matrix  $\mathbf{C}$  is tridiagonal. Then the distribution of  $\mathbf{x}^k$  converges to  $p$  geometrically fast in all coordinates, and we can couple  $\mathbf{x}^k$  and a sample  $\mathbf{z} \sim \mathcal{N}(\mathbf{m}, \mathbf{C})$  such that*

$$(2.2) \quad \mathbb{E} \|\mathbf{C}^{-1/2}(\mathbf{x}^k - \mathbf{z})\|^2 \leq \beta^k n (1 + \|\mathbf{C}^{-1/2}(\mathbf{x}^0 - \mathbf{m})\|^2),$$

where

$$(2.3) \quad \beta \leq \frac{2(1 - \mathcal{C}^{-1})^2 \mathcal{C}^4}{1 + 2(1 - \mathcal{C}^{-1})^2 \mathcal{C}^4},$$

with  $\mathcal{C}$  being the condition number of  $\mathbf{C}$ .

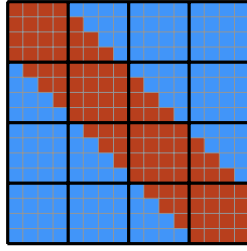


**Figure 2.1.** Sparsity pattern of a 4-block-tridiagonal matrix with bandwidth  $l = 4$ . The red color indicates nonzero entries and the blue color indicates zero entries. The black squares define the  $q = 4$  blocks  $\mathbf{C}_{i,j}$ .

Note that the upper bound for the rate of convergence  $\beta$  depends only on the condition number of the covariance matrix but is independent of the dimension. However, the upper bound itself is linear in  $n$  and involves a norm of the initial condition which may also scale linearly in  $n$ . However, this scaling does not cause practical difficulties. The dimension independent scaling of the convergence rate implies that the number of iterations required to reach a given error level scales logarithmically in  $n$ , which is essentially a constant in practice (even when  $n$  is large). For example, suppose one wants that the  $l^2$  error  $\mathbb{E}\|\mathbf{C}^{-1/2}(\mathbf{x}^k - \mathbf{z})\|^2$  be bounded by a threshold  $\epsilon$ . To reach this goal, the Gibbs sampler must perform  $k$  iterations, where

$$\beta^k n (1 + \|\mathbf{C}^{-1/2}(\mathbf{x}^0 - \mathbf{m})\|^2) \leq \epsilon \quad \Rightarrow \quad k \geq \frac{\log n - \log \epsilon + \log(1 + \|\mathbf{C}^{-1/2}(\mathbf{x}^0 - \mathbf{m})\|^2)}{-\log \beta}.$$

Finally, note that we do not use the classical total variance distance to measure convergence. We use the Wasserstein distance generated by the  $l_2$  norm. The Wasserstein metric is more suitable for analyzing high dimensional problems, where the total variance distance may be too discriminative.

**2.2. Gibbs sampling of distributions with banded covariance matrices.** We wish to consider Gaussian distributions with banded but not necessarily tridiagonal covariance matrices. To make matters precise we define the bandwidth  $l$  of a matrix  $\mathbf{C}$  by

$$l = \min\{r : [\mathbf{C}]_{i,j} = 0 \text{ if } |i - j| > r\},$$

and say that a matrix  $\mathbf{C}$  is  $q$ -block-tridiagonal, if

$$\mathbf{C}_{i,j} = \mathbf{0} \quad \text{for } (i, j) \notin \{(i, i), (i, i + 1), (i, i - 1), i = 1, \dots, m\}.$$

Here we use  $\mathbf{C}_{i,j}$  to denote the  $(i, j)$ -th  $q \times q$  block a matrix  $\mathbf{C}$ . Note that a banded matrix with bandwidth  $l$  is  $l$ -block-tridiagonal, and a  $q$ -block-tridiagonal matrix has bandwidth  $l \leq 2q$ . Figure 2.1 illustrates a 4-block-tridiagonal matrix with bandwidth  $l = 4$ . Theorem 2.1 generalizes naturally to the Gibbs sampler with block-size  $q$ . The proof of the following theorem is given in Appendix A.

**Theorem 2.2.** *Suppose the Gibbs sampler with block-size  $q$  is applied to a Gaussian target distribution  $p = \mathcal{N}(\mathbf{m}, \mathbf{C})$  with  $m$  blocks of size  $q$ . Suppose  $\mathbf{C}$  is  $q$ -block-tridiagonal. Then (2.2) as in Theorem 2.1 holds, and the convergence rate  $\beta$  is bounded as in (2.3).*

In summary, the convergence rate of a Gibbs sampler for Gaussians with (block-) tridiagonal covariance is dimension independent, and Theorem 2.2 shows that an upper bound for the convergence rate remains dimension independent if the covariance matrix is banded. Note, however, that the upper bound on the convergence rate depends on the condition number of the covariance matrix.

**2.3. Gibbs sampling of distributions with banded precision matrices.** The convergence rate of the Gibbs sampler, as described above, is also dimension-independent if the precision matrix, rather than the covariance matrix, is banded. In fact, it is straightforward to modify the above theorems to the case of banded precision matrices. For Gaussian distributions with tridiagonal precision matrix, the convergence of the Gibbs sampler is described by a variation of Theorem 2.1.

**Theorem 2.3.** *Suppose the Gibbs sampler is applied to a Gaussian target distribution  $p = \mathcal{N}(\mathbf{m}, \mathbf{\Omega}^{-1})$ , where  $\mathbf{\Omega}$  is tridiagonal. Then the distribution of  $\mathbf{x}^k$  converges to  $p$  geometrically fast in all coordinates, and we can couple  $\mathbf{x}^k$  and a sample  $\mathbf{z} \sim \mathcal{N}(\mathbf{m}, \mathbf{\Omega}^{-1})$  such that equation (2.2) holds with*

$$(2.4) \quad \beta \leq \frac{\mathcal{C}(1 - \mathcal{C}^{-1})^2}{1 + \mathcal{C}(1 - \mathcal{C}^{-1})^2},$$

where  $\mathcal{C}$  is the condition number of  $\mathbf{\Omega}$ .

For Gaussian distributions with banded precision matrix, the convergence of the Gibbs sampler with block-size  $q$  is described by a variation of Theorem 2.2.

**Theorem 2.4.** *Suppose the Gibbs sampler with block-size  $q$  is applied to a Gaussian target distribution  $p = \mathcal{N}(\mathbf{m}, \mathbf{\Omega}^{-1})$  with  $m$  blocks of size  $q$ . Suppose  $\mathbf{\Omega}$  is  $q$ -block-tridiagonal, then (2.2) as in Theorem 2.1 holds, and the convergence rate  $\beta$  is bounded as in (2.4).*

The proofs of Theorems 2.3 and 2.4 are in Appendix A.

**2.4. Banded covariance matrices vs. banded precision matrices.** Assumptions of banded covariance and precision matrix are connected. If the condition number of the covariance matrix is moderate, a banded covariance matrix implies that the precision matrix can be approximated by a banded matrix, and vice versa. This equivalence is made precise in Lemma 2.1 of [6]. Since our convergence rates depend on the condition number of the covariance matrix (or, equivalently, the precision matrix), the assumptions we make and the results we obtain apply to a unified class of problems, rather than two problem classes. As the condition number increases, the convergence rate  $\beta$  increases to (nearly) one, which makes the sampler less effective. Thus, while the convergence rate is independent of dimension, for practical applications one needs that either the covariance or precision matrix is banded *and* that the condition number is moderate. However, this means that both the covariance and precision matrix are banded, since bandedness of one implies bandedness of the other when  $\mathcal{C}$  is moderate. In other words, our results apply to Gibbs samplers for Gaussian distributions with banded covariance *and* banded precision matrices.

Finally, note that while the upper bound of the convergence rate is independent of dimension, the actual computational cost of sampling may not be independent of dimension. The

Gibbs sampler for Gaussians with banded covariance matrix requires matrix square roots and linear solves of matrices of sizes  $m \times m$  and  $d \times d$ , where  $d = n - m$ . These square roots need only be computed once (not once per sample), but the cost of this computation increases with  $n$  at a rate that depends on the bandwidth of the covariance matrix. Generating a sample requires, at each block, solution of a banded linear problem, and some matrix-vector multiplications and vector-vector operations. The cost-per-sample is dominated by the linear solve, and this cost also increases with  $n$  and at a rate that depends on the bandwidth of the covariance matrix. The computational cost for one sample is thus, roughly,  $m$  times the cost of the linear solve.

If the precision matrix is banded, however, then the conditional distributions used during Gibbs sampling simplify and it is sufficient to condition on neighboring blocks (see, e.g., equation A.1 in the appendix). The required matrix operations (square roots, linear solves) thus depend on the size of the blocks  $q$ , but not on the number of blocks. For this reason, the computational cost of Gibbs sampling for banded precision matrices is less than that of Gibbs sampling with a banded covariance matrix. Assuming that  $q \ll m \ll n$ , the computational cost of a Gibbs sampler for a Gaussian with banded precision matrix is thus, roughly,  $m$  times the cost of computations with blocks of size  $q$ .

**3. Localization of Bayesian inverse problems.** Now we consider linear inverse problems in the Bayesian setting. Let  $\mathbf{x}$  be an  $n$ -dimensional real-valued random vector. The observations are defined by

$$\mathbf{y} = \mathbf{H}\mathbf{x} + \mathbf{v},$$

where  $\mathbf{y}$  is a  $k$ -dimensional vector,  $k \leq n$ , that contains noisy versions of linear combinations of the elements of  $\mathbf{x}$ , and where  $\mathbf{H}$  is a given  $k \times n$  matrix. The observations  $\mathbf{y}$ , along with the distribution of  $\mathbf{v}$ , define a likelihood  $p_l(\mathbf{y}|\mathbf{x})$ . A prior probability distribution  $p_0$  describes prior knowledge about  $\mathbf{x}$ . For example, one may know that the variables are likely to be within a certain interval. The prior distribution often also describes the smoothness of a random field whose discretization is the vector  $\mathbf{x}$ . The prior and likelihood together define the posterior distribution

$$p(\mathbf{x}|\mathbf{y}) \propto p_0(\mathbf{x})p_l(\mathbf{y}|\mathbf{x}).$$

For the rest of this paper, we consider problems with Gaussian errors,  $\mathbf{v} \sim \mathcal{N}(\mathbf{0}, \mathbf{R})$ , and Gaussian priors  $p_0(\mathbf{x}) = \mathcal{N}(\mathbf{m}, \mathbf{C})$ . Under these assumptions, the posterior distribution is Gaussian and its mean and covariance are given by

$$\begin{aligned}\hat{\mathbf{m}} &= \mathbf{m} + \mathbf{K}(\mathbf{y} - \mathbf{H}\mathbf{x}), \\ \hat{\mathbf{C}} &= (\mathbf{I} - \mathbf{K}\mathbf{H})\mathbf{C}, \\ \mathbf{K} &= \mathbf{C}\mathbf{H}^T(\mathbf{R} + \mathbf{H}\mathbf{C}\mathbf{H}^T)^{-1},\end{aligned}$$

where  $\mathbf{K}$  is the Kalman gain. In addition, we assume that

- (i) the state dimension  $n$  is large, and  $k = O(n)$ ;

- (ii) each predicted observation  $[\mathbf{H}\mathbf{x}]_j$  depends only on  $\ell \ll n$  consecutive components of  $\mathbf{x}$ , and  $\mathbf{R}$  is diagonal.

We give a physical interpretation of our assumptions in Section 4 below.

**3.1. Localization of Bayesian inverse problems with banded covariance matrix.** In this subsection, we introduce the additional assumption that the prior covariance is nearly banded. We will make this notion more precise below, but in simple terms, nearly banded means that the elements away from the diagonal are “small.” To localize a covariance matrix is to neglect (set to zero) small off-diagonal elements. Solving a Bayesian inverse problem by localization means that we replace the original prior covariance matrix, with nearly banded structure, by a *localized* problem that has a banded prior covariance matrix. This process of covariance localization is routinely used in NWP and ensemble Kalman filtering (EnKF), where a forecast covariance is localized in precisely this way. Forecast covariance localization makes it possible to solve a problem with hundreds of millions of variables with an ensemble of (at most) a few hundred samples.

Specifically, suppose that the off-diagonal elements of the prior covariance decay away from the diagonal such that  $|\mathbf{C}_{i,j}| \geq |\mathbf{C}_{i,j+1}|$  for  $i = 1, \dots, n$ ,  $j = i, \dots, n-1$ . The prior covariance can be localized as follows. Under our assumptions,  $|\mathbf{C}_{i,j}|$  are small when  $|i-j| \geq l$  and we set these elements equal to zero. What “small” means, i.e., how to choose the threshold  $l$ , is problem dependent and  $l$  must be tuned, or determined from additional prior knowledge, as is commonly done when tuning covariance localization in NWP. The resulting localized covariance matrix  $\mathbf{C}_{\text{loc}}$  is banded and has entries

$$(3.1) \quad [\mathbf{C}_{\text{loc}}]_{i,j} = [\mathbf{C}]_{i,j} \mathbf{1}_{|i-j| \leq l},$$

where  $\mathbf{1}_{|i-j| \leq l}$  is an indicator function. The bandwidth (recall Section 2.2) of the localized covariance matrix  $\mathbf{C}_{\text{loc}}$  is less or equal to the threshold  $l$  used during localization. A localized covariance matrix is positive definite if the minimum eigenvalue of  $\mathbf{C}$  is above  $\delta_C$ , where

$$(3.2) \quad \delta_C := \max_i \sum_{j:|i-j|>l} |\mathbf{C}_{i,j}|.$$

If  $\mathbf{C}$  is nearly banded,  $\delta_C$  is small, and we show in Appendix B (Proposition B.2), that, in this case, the localized covariance matrix is a small perturbation of the covariance matrix

$$(3.3) \quad \|\mathbf{C} - \mathbf{C}_{\text{loc}}\| \leq \delta_C.$$

In summary, a nearly banded covariance matrix is one whose elements decay away from the diagonal, and a *localized* covariance matrix is banded because small off-diagonal elements are set to zero. The differences between the nearly banded and banded covariance matrices are small, as indicated by equation (3.3). We use a threshold for localization because it makes our proofs simpler. In practice, one may localize more effectively by multiplying the covariance matrix by a suitable localization function [20], which sets small off-diagonal elements to zero while maintaining positive-definiteness of the localized covariance matrix without additional assumptions on the condition number.



We can relax our assumption (ii) and can also consider observation matrices that are not strictly local, i.e., each predicted observation  $[\mathbf{H}\mathbf{x}]_j$  may depend on all components of  $\mathbf{x}$ , but the contributions of many components are negligible. In this case, the observation matrix  $\mathbf{H}$  can be localized similarly to how we localized the prior covariance. We now make this notion more precise. For a given observation matrix  $\mathbf{H}$  and a given threshold  $l_H$ , define a localized observation matrix by

$$[\mathbf{H}_{\text{loc}}]_{j,i} = [\mathbf{H}]_{j,i} \mathbb{1}_{|o_j - i| \leq l_H},$$

where  $o_j$  represents the center of the  $j$ -th observation. Following (3.2), we can quantify the difference between  $\mathbf{H}$  and  $\mathbf{H}_{\text{loc}}$  by

$$(3.4) \quad \delta_H = \max_i \left\{ \sum_{j: |i - o_j| > l_H} |[\mathbf{H}]_{j,i}|, \sum_{i: |i - o_j| > l_H} |[\mathbf{H}]_{j,i}| \right\}.$$

In analogy to nearly banded and localized prior covariance matrices, we call observation matrices with small  $\delta_H$  “nearly local,” and we propose to localize nearly local matrices by setting small elements equal to zero.

The localized prior covariance and localized observation matrix define a localized Bayesian inverse problem, characterized by a localized posterior distribution with mean and covariance given by

$$(3.5) \quad \hat{\mathbf{m}}_{\text{loc}} = \mathbf{m} + \mathbf{K}_{\text{loc}} (\mathbf{y} - \mathbf{H}_{\text{loc}} \mathbf{x}),$$

$$(3.6) \quad \hat{\mathbf{C}}_{\text{loc}} = (\mathbf{I} - \mathbf{K}_{\text{loc}} \mathbf{H}_{\text{loc}}) \mathbf{C}_{\text{loc}},$$

$$\mathbf{K}_{\text{loc}} = \mathbf{C}_{\text{loc}} \mathbf{H}_{\text{loc}}^T (\mathbf{R} + \mathbf{H}_{\text{loc}} \mathbf{C}_{\text{loc}} \mathbf{H}_{\text{loc}}^T)^{-1}.$$

We prove in Appendix B (Proposition B.2) that

$$\begin{aligned} \|\hat{\mathbf{m}} - \hat{\mathbf{m}}_{\text{loc}}\| &\leq (\delta_C + \delta_H) \cdot D_1(\|\mathbf{R}^{-1}\|, \|\hat{\mathbf{C}}\|, \|\mathbf{C}^{-1}\|) \cdot (\|\mathbf{m}\| + \|\mathbf{y}\|), \\ \|\hat{\mathbf{C}} - \hat{\mathbf{C}}_{\text{loc}}\| &\leq (\delta_C + \delta_H) \cdot D_2(\|\mathbf{R}^{-1}\|, \|\hat{\mathbf{C}}\|, \|\mathbf{C}^{-1}\|). \end{aligned}$$

Thus, the mean and covariance of the localized problem are small perturbations of the posterior mean and covariance, if  $\mathbf{C}$  is nearly banded and  $\mathbf{H}$  is nearly local, i.e., if  $\delta_C$  and  $\delta_H$  are small.

Note that the difference between the localized and unlocalized problems depends on the localization thresholds we chose, on the structure of the prior covariance matrix, and the observation matrix  $\mathbf{H}$ . The bandwidth of localizations of  $\mathbf{C}$  and  $\mathbf{H}$  should therefore be tuned to obtain small differences. The motivation for localization is that we can exploit banded covariances and local observations during sampling, as explained below, and, thus, trade numerical efficiency against errors which can be controlled (errors vanish when the localization thresholds are sufficiently small).

**3.1.1. Localized Metropolis-within-Gibbs sampling: banded covariance.** We now present a localized Metropolis-within-Gibbs (l-MwG) sampler whose stationary distribution is the localized posterior distribution. Suppose the prior covariance matrix is block-tridiagonal, with  $m$  blocks of size  $q$ , and further suppose that  $\mathbf{x}^k$ , is the current state of a Markov chain.

One iteration of the l-MwG sampler is as follows. Start with the first of  $m$  blocks. Use the Gibbs proposal with block-size  $q$  (see Section 2.2) to propose a local move  $\mathbf{x}'$  by drawing a sample from the Gaussian prior, conditioned on the current state  $\mathbf{x}^k$ . Accept the move using a local accept/reject criterion that takes into account the observations in the neighborhood of the given block, rather than all observations (see below). Iterating these steps over all  $m$  blocks completes one move of the l-MwG.

The local accept/reject step is as follows. We assign the elements of the observations  $\mathbf{y}$  to the various blocks within the localized prior covariance  $\mathbf{C}_{\text{loc}}$ . For simplicity we first consider the case with one observation per block. A local move is accepted with probability

$$(3.7) \quad a = \max \left( \frac{\exp(-0.5(y_j - [\mathbf{H}_{\text{loc}}\mathbf{x}']_j)^T [\mathbf{R}]_{j,j}^{-1} (y_j - [\mathbf{H}_{\text{loc}}\mathbf{x}']_j))}{\exp(-0.5(y_j - [\mathbf{H}_{\text{loc}}\mathbf{x}]_j)^T [\mathbf{R}]_{j,j}^{-1} (y_j - [\mathbf{H}_{\text{loc}}\mathbf{x}]_j))}, 1 \right),$$

where  $y_j$  is the observation corresponding to the current block;  $[\mathbf{R}]_{j,j}$  is the  $j$ th diagonal entry of  $\mathbf{R}$ , and  $[\mathbf{H}_{\text{loc}}\mathbf{x}]_j$  is the  $j$ th element of  $\mathbf{H}_{\text{loc}}\mathbf{x}$ ; we drop the time-index  $k$  for readability.

More generally, the localized posterior distribution can be written as

$$(3.8) \quad p_{\text{loc}}(\mathbf{x}|\mathbf{y}) \propto p_{0,\text{loc}}(\mathbf{x}) \exp \left( - \sum_j H_j(\mathbf{x}_{I_j}, \mathbf{y}_j) \right),$$

where  $\mathbf{x}_{I_j}$  is the set of variables assigned to the observations  $\mathbf{y}_j$ , and where  $p_{0,\text{loc}} = \mathcal{N}(\mathbf{m}, \mathbf{C}_{\text{loc}})$  is the localized prior distribution. Each local update generates a new sample  $\mathbf{x}'$  from  $\mathbf{x}$  with transition density  $K_i(\mathbf{x}, \mathbf{x}')$ , defined by the Gibbs move, such that  $\mathbf{x}_j = \mathbf{x}'_j$  for  $j \neq i$ , and  $p_{0,\text{loc}}(\mathbf{x})$  is the invariant distribution of this transition, in the sense that

$$p_{0,\text{loc}}(\mathbf{x})K_i(\mathbf{x}, \mathbf{x}') = p_{0,\text{loc}}(\mathbf{x}')K_i(\mathbf{x}', \mathbf{x}).$$

The proposed local adjustment of the sample,  $\mathbf{x}'$ , is accepted with probability

$$(3.9) \quad \max \left\{ 1, \frac{\exp(-\sum_{j:i \in I_j} H_j(\mathbf{x}'_{I_j}, \mathbf{y}_j))}{\exp(-\sum_{j:i \in I_j} H_j(\mathbf{x}_{I_j}, \mathbf{y}_j))} \right\}.$$

The stationary distribution of the l-MwG sampler is the localized posterior distribution

$$p_{\text{loc}}(\mathbf{x}|\mathbf{y}) = \mathcal{N}(\hat{\mathbf{m}}_{\text{loc}}, \hat{\mathbf{C}}_{\text{loc}}),$$

with mean and covariance given by equations (3.5) and (3.6). To prove this statement, it suffices to check the detailed balanced relation

$$p_{\text{loc}}(\mathbf{x}|\mathbf{y})Q_i(\mathbf{x}, \mathbf{x}') = p_{\text{loc}}(\mathbf{x}'|\mathbf{y})Q_i(\mathbf{x}', \mathbf{x})$$

for  $\mathbf{x} \neq \mathbf{x}'$ , where  $Q_i$  is the transition density resulting from the above two steps (propose a local sample using the Gibbs proposal for the prior, then accept or reject it using the local criterion (3.9)). For  $\mathbf{x} \neq \mathbf{x}'$ , the transition density has the explicit form:

$$Q_i(\mathbf{x}, \mathbf{x}') = K_i(\mathbf{x}, \mathbf{x}') \max \left\{ 1, \frac{\exp(-\sum_{j:i \in I_j} H_j(\mathbf{x}'_{I_j}, \mathbf{y}_j))}{\exp(-\sum_{j:i \in I_j} H_j(\mathbf{x}_{I_j}, \mathbf{y}_j))} \right\}.$$

Without loss of generality, we assume  $\sum_{j:i \in I_j} H_j(\mathbf{x}'_{I_j}, \mathbf{y}_j) \leq \sum_{j:i \in I_j} H_j(\mathbf{x}_{I_j}, \mathbf{y}_j)$  which leads to

$$p_{\text{loc}}(\mathbf{x}|\mathbf{y})Q_i(\mathbf{x}, \mathbf{x}') = p_{0,\text{loc}}(\mathbf{x})K_i(\mathbf{x}, \mathbf{x}') \exp\left(-\sum_{j:i \in I_j} H_j(\mathbf{x}_{I_j}, \mathbf{y}_j)\right),$$

$$p_{\text{loc}}(\mathbf{x}'|\mathbf{y})Q_i(\mathbf{x}', \mathbf{x}) = p_{0,\text{loc}}(\mathbf{x}')K_i(\mathbf{x}', \mathbf{x}) \exp\left(-\sum_{j:i \in I_j} H_j(\mathbf{x}_{I_j}, \mathbf{y}_j)\right) \frac{\exp(-\sum_{j:i \in I_j} H_j(\mathbf{x}_{I_j}, \mathbf{y}_j))}{\exp(-\sum_{j:i \in I_j} H_j(\mathbf{x}'_{I_j}, \mathbf{y}_j))}.$$

Because we also have that

$$p_{0,\text{loc}}(\mathbf{x})K_i(\mathbf{x}, \mathbf{x}') = p_{0,\text{loc}}(\mathbf{x}')K_i(\mathbf{x}', \mathbf{x}), \quad \mathbf{x}'_j = \mathbf{x}_j \quad \forall j \neq i,$$

detailed balance, i.e.,  $p_{\text{loc}}(\mathbf{x}|\mathbf{y})Q_i(\mathbf{x}, \mathbf{x}') = p_{\text{loc}}(\mathbf{x}'|\mathbf{y})Q_i(\mathbf{x}', \mathbf{x})$ , is now verified.

**3.2. Localization of Bayesian inverse problems with banded precision matrices.** Working with prior precision matrices, rather than prior covariance matrices, is sometimes more natural. In this case, one can write the prior distribution as  $p_0(\mathbf{x}) = \mathcal{N}(\mathbf{m}, \mathbf{\Omega}^{-1})$ , where  $\mathbf{\Omega}$  is the prior precision matrix. The likelihood is as before, i.e.,  $p_l(\mathbf{y}|\mathbf{x}) = \mathcal{N}(\mathbf{H}\mathbf{x}, \mathbf{R})$ , and the posterior distribution is  $p(\mathbf{x}|\mathbf{y}) \propto p_0(\mathbf{x})p_l(\mathbf{y}|\mathbf{x})$ .

The framework of localization can be adapted to this case because precision matrices can be localized in the same way as covariance matrices, if the elements of the precision matrix decay away from the diagonal. Assuming, as before, that the observation matrix  $\mathbf{H}$  is local (see assumption (ii)), or can be localized, one obtains a localized Bayesian inverse problem, which is a small perturbation of the unlocalized problem and whose localized posterior distribution can be sampled efficiently by l-MwG. We now describe this process in more detail.

Localizing a prior precision matrix amounts to setting small off-diagonal elements to zero, which does not introduce large additional errors if the off-diagonal elements are small, e.g., if the elements  $|\mathbf{\Omega}_{i,j}|$ , are nearly zero when  $|i-j| > l$  for a threshold  $l$ . All elements that are smaller than the threshold are set to zero which results in a banded prior precision matrix (each row consists of at most  $2l$  nonzero entries). The entries of this matrix are  $[\mathbf{\Omega}_{\text{loc}}]_{i,j} = [\mathbf{\Omega}]_{i,j} \mathbb{1}_{|i-j| \leq l}$ . Moreover, we show in Appendix B, Proposition B.3, that the localized covariance matrix is a small perturbation of the covariance matrix:

$$(3.10) \quad \|\mathbf{\Omega} - \mathbf{\Omega}_{\text{loc}}\| \leq \delta_{\Omega}, \quad \delta_{\Omega} := \max_i \sum_{j:|i-j|>l} |[\mathbf{\Omega}]_{i,j}|.$$

Localization of the precision matrix results in a localized prior distribution  $p_{0,\text{loc}} = \mathcal{N}(\mathbf{m}, \mathbf{\Omega}_{\text{loc}}^{-1})$ . The observation matrix  $\mathbf{H}$  can be localized as before (see Section 3.1), which gives  $\mathbf{H}_{\text{loc}}$  and defines a localized likelihood  $p_{l,\text{loc}}(\mathbf{y}|\mathbf{x}) = \mathcal{N}(\mathbf{H}_{\text{loc}}\mathbf{x}, \mathbf{R})$ . The mean and covariance of the localized posterior are given by

$$\begin{aligned} \hat{\mathbf{m}}_{\text{p,loc}} &= \mathbf{m} + \mathbf{K}_{\text{p,loc}}(\mathbf{y} - \mathbf{H}_{\text{loc}}\mathbf{x}), \\ \hat{\mathbf{C}}_{\text{p,loc}} &= (\mathbf{I} - \mathbf{K}_{\text{p,loc}}\mathbf{H}_{\text{loc}})\mathbf{\Omega}_{\text{loc}}^{-1}, \\ \mathbf{K}_{\text{p,loc}} &= \mathbf{\Omega}_{\text{loc}}^{-1}\mathbf{H}_{\text{loc}}^T(\mathbf{R} + \mathbf{H}_{\text{loc}}\mathbf{\Omega}_{\text{loc}}^{-1}\mathbf{H}_{\text{loc}}^T)^{-1}. \end{aligned}$$

The mean and covariance of the localized posterior distribution are small perturbations of the mean and covariance matrix of the unlocalized posterior distribution:

$$\begin{aligned}\|\hat{\mathbf{m}} - \hat{\mathbf{m}}_{\text{p,loc}}\| &\leq (\delta_\Omega + \delta_H) \cdot D_3(\|\mathbf{R}^{-1}\|, \|\hat{\mathbf{C}}\|, \|\boldsymbol{\Omega}\|) \cdot (\|\mathbf{m}\| + \|\mathbf{y}\|), \\ \|\hat{\mathbf{C}} - \hat{\mathbf{C}}_{\text{p,loc}}\| &\leq (\delta_\Omega + \delta_H) \cdot D_4(\|\mathbf{R}^{-1}\|, \|\hat{\mathbf{C}}\|, \|\boldsymbol{\Omega}\|).\end{aligned}$$

Similar perturbations of the posterior precision matrix, i.e.,  $\|\hat{\mathbf{C}}^{-1} - \hat{\mathbf{C}}_{\text{p,loc}}^{-1}\|$ , can also be derived. The explicit dependence of  $D_3$  and  $D_4$  on  $\|\mathbf{R}^{-1}\|, \|\hat{\mathbf{C}}\|, \|\mathbf{C}^{-1}\|$  can be found in Appendix B (Proposition B.3). Thus, as in the earlier case of covariance localization, localizing the precision matrix introduces bias, but this bias is small under suitable assumptions and is controllable by the choice of bandwidth for the localization.

**3.2.1. Localized Metropolis-within-Gibbs sampling: banded precision.** The l-MwG sampler of Section 3.1.1 can be applied to the precision-localized inverse problem. The procedure is as described above, but the implementation using precision matrices can be numerically more efficient. If the precision matrix has bandwidth  $l$ , then the conditional distribution of a block depends only on a few neighboring blocks, so that the computations required for drawing a sample from the conditional distributions require only matrices of size much less than  $n$  (see also Section 2.4, and equation A.1 in the appendix). As an example, consider a localized prior distribution  $\mathcal{N}(\mathbf{m}, \boldsymbol{\Omega}^{-1})$  whose localized precision matrix has block size  $q \geq l$ . In this case, the probability of  $\mathbf{x}_j$  conditioned on all other blocks is the same as the probability of  $\mathbf{x}_j$  conditioned on its two neighboring blocks:

$$p(\mathbf{x}_j | \mathbf{x}_1, \dots, \mathbf{x}_{j-1}, \mathbf{x}_{j+1}, \dots, \mathbf{x}_m) = p(\mathbf{x}_j | \mathbf{x}_{j-1}, \mathbf{x}_{j+1}).$$

The conditional independence also implies that one can sample far-away blocks independently. In our above example, sampling from  $p(\mathbf{x}_{2j+1} | \mathbf{x}_{2j}^k, \mathbf{x}_{2j+2}^k)$  can be done independently of sampling from  $p(\mathbf{x}_{2i+1} | \mathbf{x}_{2i}^k, \mathbf{x}_{2i+2}^k)$ , if  $i \neq j$ . This provides opportunities for leveraging advantages of parallel computing to reduce overall wall-clock time.

**3.3. Computational requirements of l-MwG.** Recall that the convergence rate of the Gibbs sampler for the localized prior is independent of dimension (Theorem 2.2). The acceptance ratio in equation (3.7) depends only on the number of observations within each block, but is also independent of dimension, or the overall number of observations. Our assumption of  $k = O(n)$  implies that the number of observations grows with the dimension, but the density of observations remains fixed. Therefore, the acceptance ratio does not change with dimension. Moreover, the size of the proposed moves does not decrease as we increase dimension, since the size of the move depends only on the properties of one of the blocks, rather than the overall number of blocks. Thus, neither the acceptance ratio nor the size of the proposed moves deteriorate as dimension and number of observations increase. For these reasons, one can expect that the convergence rate of the l-MwG sampler is independent of dimension, and that indicators of sampling efficiency, e.g., IACT, depend only on the properties of the blocks within the prior, rather than on the number of blocks. We cannot provide a formal proof for the dimension independence of l-MwG, but we will provide numerical examples in which IACT is indeed independent of dimension, while IACT increases with dimension for other

MCMC algorithms. We also present an example in which we deliberately violate some of our assumptions to demonstrate the limitations of our ideas.

Finally, note that, under our assumptions, the posterior covariance matrix is nearly banded, because, as shown in [6], basic arithmetic operations in (3.6) preserve matrix finite-bandedness. One can thus envision another computational route to solving this problem, which consists of explicitly computing the mean and banded covariance of the localized posterior, and then applying the Gibbs sampler of Section 2 to that distribution. Indeed, the convergence rate of the Gibbs sampler is independent of dimension in this case. For Gaussian problems (at least of moderate size) this may be a good approach that can exploit sparse linear algebra. However, the approach requires that one first computes the posterior mean and posterior covariance, and does not easily generalize to nonlinear or non-Gaussian problems. In contrast, a modification of the above l-MwG sampler to non-Gaussian problems is straightforward.

#### 4. Discussion.

**4.1. Physical interpretation of our assumptions.** Our assumptions correspond to prior distributions with short correlation lengths (e.g., in a Gaussian process) and small neighborhood sizes (e.g., in a Gaussian Markov random field [47]) relative to the dimensions of the physical domain. The priors are updated to posterior distributions by likelihoods involving observations that depend largely on local properties. We expect that these assumptions are valid in many geophysical and engineering applications of MCMC, where the target distribution is the posterior distribution of a physical quantity defined over some spatial domain. A common choice of prior distribution is a Gaussian with precision matrix defined via a ‘‘Laplace-like’’ operator; see, e.g., [8, 14, 30, 33, 38, 50] and our examples below. These priors typically have banded precision matrices and, in many cases, also have (nearly) banded covariance matrices.

The observation matrix is local if the ‘‘quantity of interest’’  $\mathbf{x}$  is directly observed, which is the case in many state estimation problems. Observation matrices in image deblurring are often constructed through the discretization of kernels that have (nearly) compact support, and, for that reason, are also typically local or nearly local. Observations of diffusion processes are local on sufficiently short time scales. Also, PDEs where information is carried mostly along characteristics (e.g., transport equations) give rise to local observations when the quantity of interest is an initial condition. The opposite, however, may also be true: in computed tomography, each observation might depend on material properties along an entire tomographic ray, leading to observation matrices which are not at all local. Localization, and the algorithms we discuss here, are not useful for such problems.

Numerical evidence that the banded covariance and precision structure we assume is common can be found in the NWP literature. A banded covariance structure is routinely assumed and used in applications of the EnKF [16, 51]. During a typical EnKF step, the covariance of  $10^8$  grid points needs to be estimated accurately, but the number of samples used is usually 100 or less [32]. This seemingly impossible task is made possible by exploiting banded covariance structure of the NWP problem. During forecast covariance localization [24–26], a banded structure is imposed on the sample covariance matrix by multiplying each entry of the covariance with a suitable localization function, e.g., the one in [20]. During this localization small off-diagonal elements are set to zero. Practitioners agree that localization is required

to make EnKF applicable to large-scale NWP problems. Indeed, the fact that EnKF works so well, in the sense that it produces useful forecasts, is an indication that the NWP problem indeed has the assumed banded structure [34]. From a more theoretical perspective, it was shown in [5] that one can estimate a localized covariance matrix with bandwidth  $l$  with  $O(l + \log n)$  samples. Reference [53] provides detailed explanations of how this result is used in the context of EnKF. Exploiting banded problem structure in importance sampling, or particle filtering, is also a current topic in NWP, and first ideas in this direction can be found in several papers, e.g., [28, 29, 37, 39–43, 52, 54].

#### 4.2. Connections with infinite dimensional inverse problems and effective dimensions.

As indicated above, one can think of  $\mathbf{x}$  as a physical quantity defined on a grid over a given domain. Its dimension,  $n$ , grows as the grid is refined. When we keep the number of observations,  $k$ , constant, and let  $n \rightarrow \infty$ , then we describe what happens as the grid is refined, while the domain and observation network remain fixed. This leads to the concept of an effective dimension, which may be small (finite) even when the apparent dimension is large (infinite); see, e.g., [1, 9].

Related to a small effective dimension are “low-rank updates” from prior to posterior distributions [13, 17, 49]. A low-rank update means that the posterior distribution differs from the prior distribution in  $n_{\text{eff}} \ll n$  directions. More precisely, for Gaussian problems, a low-rank update means that the difference between prior and posterior covariance is low rank. In practice this occurs, for example, when the number of observations is much less than the parameter dimension, or when the observations constrain only a few linear combinations of the parameters. Indeed, some definitions of effective dimension are directly related to the difference of prior and posterior covariance. In [1], an effective dimension is defined by:

$$n_{\text{eff},1} = \text{tr}((\mathbf{C} - \hat{\mathbf{C}})\mathbf{C}^{-1}),$$

where  $\mathbf{C}$  and  $\hat{\mathbf{C}}$  are prior and posterior covariance and where  $\text{tr}(\mathbf{A})$  is the trace of a matrix  $\mathbf{A}$ . Alternatively, one can consider precision matrices and define an effective dimension by

$$n_{\text{eff},2} = \text{tr}((\hat{\mathbf{\Omega}} - \mathbf{\Omega})\mathbf{\Omega}^{-1}),$$

where  $\mathbf{\Omega}$  and  $\hat{\mathbf{\Omega}}$  are the prior and posterior precision matrices. Other effective dimensions can be defined for specific importance sampling or MCMC algorithms; see, e.g., [1, 9]. Certain MCMC and importance sampling algorithms can exploit a small effective dimension or low rank updates, and can be made discretization invariant—such that indicators of computational efficiency become independent of the chosen grid; see, e.g., [8, 11, 12, 17, 38].

Our assumptions and problem setting describe a different mechanism for large dimension because we assume that the number of observations is on the order of the dimension,  $k = O(n)$ . The assumptions translate to a problem for which the discretization and observation density remain fixed, while the size of the domain grows. As an example, consider a Gaussian process defined on an interval of length  $L$ . Further suppose that this process is measured every  $r$  units of distance, i.e., we have  $L/r$  observations. We investigate the situation where the interval, or domain size  $L$ , gets bigger, but the number of observations per unit length remains constant. The limit  $n \rightarrow \infty$  may not be meaningful because it would correspond to an infinitely large

domain. Considering large  $n$ , however, is meaningful because it describes a large domain and a large number of observations. The scaling of performance indicators of MCMC with  $n$  (and  $k$ ) indicates how MCMC algorithms perform on problems over large, well observed, physical domains. The cartoon example in the introduction, i.e., sampling a high-dimensional isotropic Gaussian, illustrates the performance one can expect from MCMC when the size of the domain is large, and the number of observations is on the order of the dimension. Moreover, our assumptions do not necessarily imply that updates from prior to posterior are low-rank. Rather, we replace assumptions about low effective dimension and/or low-rank updates by assumptions about bandedness of the precision and covariance matrices and local observations. The MCMC algorithms we describe are efficient when precision and covariance matrices are banded, and if observations are local. If our assumptions are only approximately satisfied, we propose to replace covariance/precision matrices by banded matrices in a process called “localization.” The resulting, localized, problem can be solved efficiently, but at the cost of additional errors due to the localization procedure.

In summary, we conclude that MCMC for generic high-dimensional problems remains difficult, but one can effectively solve two classes of problems. If an effective dimension is small and/or an update from prior to posterior distribution is low-rank, then one can exploit this structure and create effective MCMC algorithms. This case has been discussed extensively over the past years. Our main contribution is to suggest that MCMC can also be made efficient if the covariance and precision matrices are banded. In fact, the situation we describe is analogous to linear algebra. High-dimensional matrices are easy to deal with if they are either low-rank or banded (sparse). The same seems true in MCMC for Bayesian inverse problems—these problems are manageable if either an effective dimension is small, or if the covariance and precision matrices have banded structure.

## 5. Numerical illustrations.

**5.1. Example 1: Gaussian prior with exponential covariance function.** We consider a Gaussian prior on the interval  $z \in [0, L]$  with mean and covariance function

$$\mu(z) = 5 \sin(2\pi z), \quad k(z, z') = C \exp\left(-\frac{|z - z'|}{2\rho}\right).$$

This results in a slowly varying prior mean and, for a given discretization, the covariance matrix has off-diagonal elements that decay quickly away from the diagonal. We consider the case with  $\rho = 0.02$ ,  $C = 10$ , and fix a discretization of the domain with  $\Delta z = 0.01$ . For a given domain size  $L$ , the dimension of the discretized Gaussian is  $n = L/\Delta z$ , i.e., we have 100 state variables per unit length. For numerical stability we add  $10^{-6} \mathbf{I}$  to the discretized covariance matrix. Samples from the prior are shown (in teal) for a problem with  $L = 3$  in Figure 5.1. The data are measurements of a prior sample, collected every  $2\Delta z$  length units. The measurements are perturbed by Gaussian noise with mean zero and identity covariance matrix, i.e.,  $\mathbf{R} = \mathbf{I}$ , the identity matrix of size  $n/2$ . Note that the observation network is such that no localization of the observation matrix  $\mathbf{H}$  is required, because the observations are already local (point-wise measurements and diagonal  $\mathbf{R}$ ). For a given  $L$  we have  $n$  variables to estimate and  $n/2$  data points, or, equivalently, we have 100 variables and 50 measurements per unit length. The true state and measurements are illustrated (in orange) for a problem with  $L = 3$  in Figure 5.1.

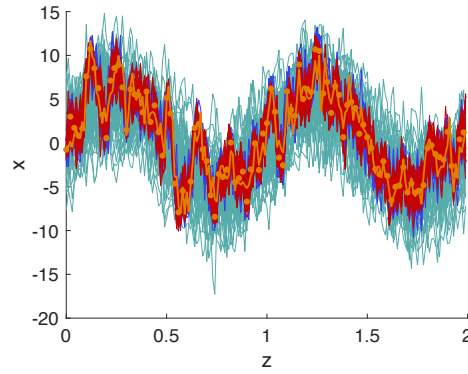


**Figure 5.1.** Illustration of the Gaussian inverse problem of example 1. Teal – 50 samples of the prior distribution. Red – 50 samples of l-MwG. Blue (often hidden) – 50 samples of posterior distribution. Orange line – “true state” that gives rise to the data. Orange dots – data.

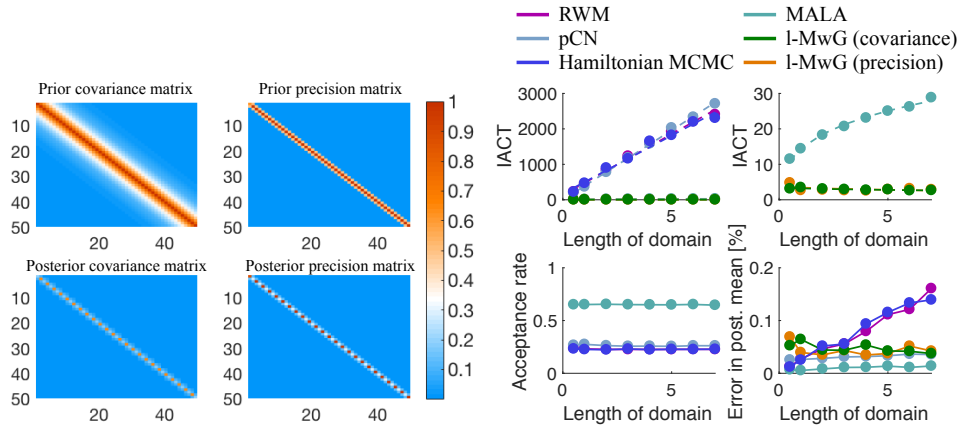


**Figure 5.2.** Covariance and precision matrices, IACT, acceptance rate and errors for Example 1. Left panels. Prior and posterior covariance and precision matrices of example 1 with  $L = 0.5$ . Top row: prior covariance (left) and precision matrix (right). Bottom row: posterior covariance (left) and precision matrix (right). Right panels. Top row: IACT as a function of domain length for RWM, pCN, Hamiltonian MCMC (left) and MALA and l-MwG (right). Bottom row: acceptance rate as a function of domain length (left) and mean squared error in posterior mean (right).

The data and prior distribution define a Bayesian posterior distribution, and we show 50 samples of this posterior distribution (for  $L = 3$ ) in Figure 5.1.

To illustrate the banded structure and relative size of the elements of the prior and posterior covariance/precision matrices, we plot the absolute value of the elements of these matrices, scaled by their largest element, in the left panels of Figure 5.2. These scaled absolute values are between 0 and 1, and indicate where off-diagonal elements are small. The prior and posterior covariance matrix have nearly banded structure in the sense that the elements near the diagonal are larger than the off-diagonal elements. This structure is exploited during covariance localization by setting small off-diagonal elements of the covariance matrix equal to zero. In the numerical experiments below we use a threshold of 0.1 for covariance localization. The



Algorithm	Step-size	Sample size	IACT scaling
RWM	$n^{-1/2}, n^{-1/2}, n^{-1/2}$	$10^6, 10^6, 10^6$	$n, n, n$
MALA	$n^{-1/3}, n^{-1/2}, n^{-1/2}$	$10^4, 10^4, 10^4$	$n^{1/4}, n^{1/4}, n^{1/4}$
Hamiltonian MCMC	$n^{-1/2}, n^{-1/2}, n^{-1/3}$	$10^5, 10^5, 10^5$	$n, n, n$
pCN	$n^{-1/2}, n^{-1/2}, n^{-1/3}$	$10^6, 10^6, 10^6$	$n, n, n$
l-MwG (precision)	n/a	500, 500, 5000	const., const., $n^{1/2}$
l-MwG (covariance)	n/a	500, 500, 5000	const., const., $n^{1/2}$

Table 1

Configurations and IACT scalings for examples 1, 2 and 3. In each cell, left to right, are the configurations and results for examples 1, 2 and 3.

prior precision matrix is tridiagonal, which is used in the lMwG sampler in “precision matrix implementation,” by conditioning on neighbors, rather than the full state. In summary, the l-MwG sampler with covariance localization does not generate samples from the posterior distribution defined by the Bayesian inverse problem above, but rather of a nearby posterior distribution, defined by the localized Bayesian inverse problem. The l-MwG sampler generates samples from the “true” posterior because the precision matrix is tridiagonal and does not require localization. The condition number of the prior precision and covariance matrices is about 64 (independently of the domain length).

For a fixed domain length  $L$ , we apply RWM, pCN, MALA, Hamiltonian MCMC and l-MwG (with covariance localization or in precision matrix implementation). We tune the step-size for RWM, pCN, MALA, Hamiltonian MCMC by considering a scaling of the step-size with  $n^{-1}, n^{-1/2}, n^{-1/3}$  and  $n^{-1/4}$  and call the step-size leading to the smallest IACT “optimal” (recall that the dimension of our discretization is  $n = L/\Delta z$ ). All chains are initialized by a random sample from the prior and we produce  $10^6$  samples with pCN,  $10^6$  with RWM,  $10^5$  with Hamiltonian MCMC,  $10^3$  with MALA, and 500 with the l-MwG samplers. The set-up for this problem is also summarized in Table 1.

We perform numerical experiments for domain lengths ranging from  $L = 0.5$  to  $L = 7$ , which leads to problems of dimension  $n = 50$  to  $n = 700$ , and with 25 to 350 observations. For each domain length and algorithm we compute the corresponding IACT. This leads to the scalings, obtained by least-squares fitting of polynomials, of IACT with dimension, as shown in Table 1, and as illustrated in Figure 5.2. We observe that RWM, pCN, Hamiltonian MCMC and MALA exhibit an increasing IACT (at different rates) as the domain size and the number of observations increase, while both implementations of l-MwG are characterized by an IACT that remains constant.

We further compute the acceptance rate (i.e., the acceptance ratio, averaged over all moves) for RWM, pCN, Hamiltonian MCMC and MALA. Results are shown in Figure 5.2, and we note that our tuning of the step-size for each algorithm keeps the acceptance rate constant as dimension increases. Finally, we compute an error to check that each algorithm indeed samples the correct distribution. We define an “error in posterior mean” by

$$(5.1) \quad e = \frac{1}{n} \sum_{j=1}^n ([\hat{\mathbf{m}}]_j - [\bar{\mathbf{x}}]_j)^2,$$

where  $\hat{\mathbf{m}}$  is the posterior mean and where  $\bar{\mathbf{x}}$  is the average over the MCMC samples. We compute this error, which describes how far our estimated posterior mean is from the actual posterior mean, for each algorithm and show the results in Figure 5.2. We note that all algorithms lead to a small error. Since this is also true for l-MwG with covariance localization, we conclude that the localized problem is indeed nearby the unlocalized problem we set out to solve.

For this problem with tridigaonal precision matrix, l-MwG in precision matrix implementation is exact, i.e., this sampler generates samples from the posterior distribution. The l-MwG sampler in covariance matrix implementation solves a localized problem because we set small off-diagonal elements of the prior covariance matrix equal to zero. The localized problem is a small perturbation of the unlocalized problem so that estimates of the posterior mean of the localized problem are good approximations of the mean of the unlocalized problem. In this example, it is not the overall dimension or the overall number of observations, or the rank of the update of prior to posterior covariance matrix that defines performance bounds for MCMC. If the banded structure is used during problem formulation and during its solution, then the characteristics of each loosely coupled block of variables are important, but the overall number of blocks is irrelevant.

**5.2. Example 2: Gaussian prior with squared Laplacian as precision matrix.** We now consider a Gaussian prior on  $z \in [0, L]$  with mean zero and with a precision matrix derived from the squared Laplacian, which leads to a pentadiagonal precision matrix after discretization. As before, we fix the discretization and chose  $\Delta z = 0.01$ . The Laplacian is approximated by the  $n = L/\Delta z$  dimensional matrix  $\mathbf{L} = 1/(\Delta z)^2 \mathbf{A}$ , where  $\mathbf{A}$  is a matrix with 2 on the main diagonal and  $-1$  on the first upper and lower diagonal. We define the precision matrix by  $\mathbf{\Omega} = (1/\rho^2 \mathbf{I} + \mathbf{L})^2$ , where  $\rho = 0.06$ . As in example 1, we collect data by collecting noisy measurements of a prior sample every  $L/(2\Delta z)$  units. The data are perturbed by a Gaussian random variable with mean zero and covariance  $\mathbf{R} = \mathbf{I}$ . As in Example 1, the discretization and observation network yields 100 discrete state variables and 50 data points per unit length. The condition number of the prior precision or covariance matrix is about  $21 \cdot 10^3$ .

In Figure 5.3, we illustrate the banded structure of the prior and posterior covariance and precision matrices for a problem with domain length  $L = 0.5$ . As in example 1, the prior precision and covariance matrices are banded, i.e., the diagonal elements are much larger than the off-diagonal elements. However, we note that the bandwidths of prior and posterior covariance matrices are larger than the bandwidths of the prior and posterior precision matrices. In particular, the prior precision matrix is pentadiagonal. The l-MwG sampler in precision matrix implementation can make use of this structure and we condition only on the five nearest neighbors (on either side), rather than all other variables. The l-MwG sampler in covariance matrix implementation requires localization and we set the localization threshold to 0.01. We also apply RMW, pCN [11], MALA, Hamiltonian MCMC, and tune their step-size as described in Example 1 above, with our findings summarized in Table 1. The number of samples we consider for each algorithm is also given in Table 1.

We vary the domain length  $L$  from  $L = 0.5$  to  $L = 7$ , apply the various samplers and compute the corresponding IACTs. This leads to the scalings of IACT with domain length (or, equivalently, dimension) as shown in Table 1, and as illustrated in Figure 5.3. While

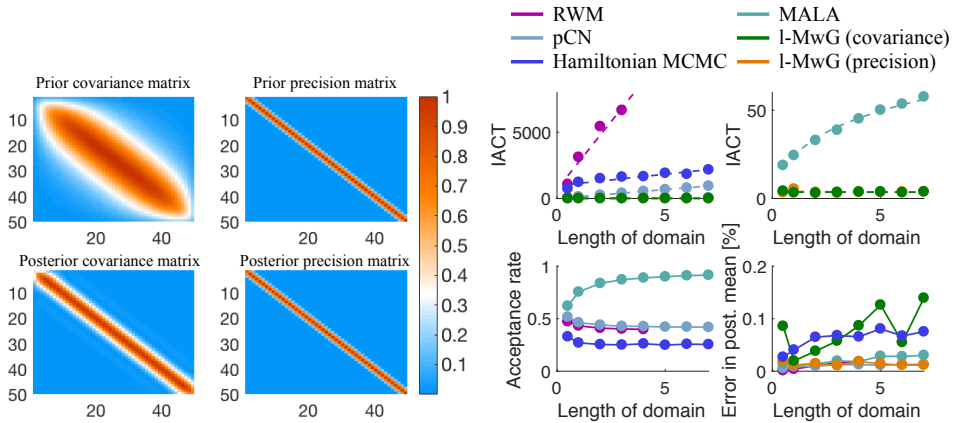


**Figure 5.3.** Covariance and precision matrices, IACT, acceptance rate and errors for Example 2. Left panels. Prior and posterior covariance and precision matrices of Example 2 with  $L = 0.5$ . Top row: prior covariance (left) and precision matrix (right). Bottom row: posterior covariance (left) and precision matrix (right). Right panels. Top row: IACT as a function of domain length for RWM, pCN, Hamiltonian MCMC (left) and MALA and l-MwG (right). Bottom row: acceptance rate as a function of domain length (left) and mean squared error in posterior mean (right).

the scalings of IACT with domain size for RWM, Hamiltonian MCMC and pCN are equal (all scale linearly), we find that IACT of pCN and Hamiltonian MCMC is reduced compared to RWM. As in Example 1, we find that the l-MwG samplers and MALA exhibit smaller IACT than the other algorithms we tested, and that IACT of the l-MwG samplers remains constant as we increase the domain length. We further find that the acceptance rate of MALA first increases with  $L$ , but then levels off (due to our tuning of the step-size). Similarly, the acceptance rate of RWM, pCN, and Hamiltonian MCMC first decreases, but then levels off for large  $L$ . All algorithms yield a small error (see  $e$  in equation (5.1), which, in the case of l-MwG in covariance matrix implementation, supports the claim that the localized problem is indeed a small perturbation of the unlocalized problem.

**5.3. Example 3: banded covariance, but full precision matrix.** We now consider a discrete Gaussian prior and Gaussian inverse problem that does not necessarily have a limit as the discretization is refined. We pick this perhaps unphysical problem to illustrate limitations of l-MwG when the condition number is large and when it increases with dimension.

We pick a dimension,  $n$ , and chose a zero mean and a covariance matrix given by an  $n \times n$  matrix  $\mathbf{C}$  which has 2 on the main diagonal and  $-1$  on the first upper and lower diagonal. We vary the dimension between  $n = 50$  and  $n = 700$  which leads to condition numbers between  $1 \cdot 10^3$  and  $2 \cdot 10^5$  (the condition number strictly increases with dimension). Because of the large condition number, the banded covariance does not imply that the precision matrix is also banded. In fact, for this prior, the covariance matrix is tridiagonal, but the precision matrix is full, as illustrated in Figure 5.4. As in examples 1 and 2, we observe every other variable and perturb these measurements by a Gaussian with mean zero and covariance  $\mathbf{R} = \mathbf{I}$ , where  $\mathbf{I}$  is the identity matrix of dimension  $n/2$ . Because the prior precision matrix is not banded, the posterior precision is also not banded as shown in Figure 5.4.

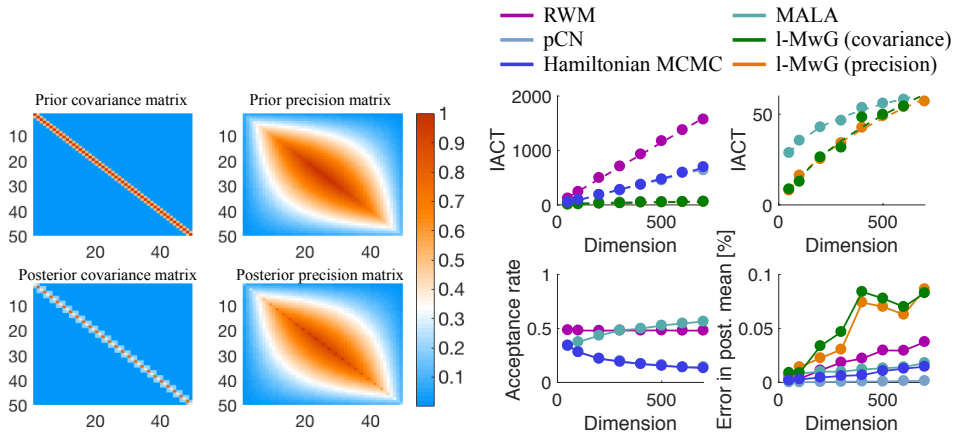


**Figure 5.4.** Covariance and precision matrices, IACT, acceptance rate and errors for Example 3. Left panels. Prior and posterior covariance and precision matrices of Example 3 with  $L = 0.5$ . Top row: prior covariance (left) and precision matrix (right). Bottom row: posterior covariance (left) and precision matrix (right). Right panels. Top row: IACT as a function of domain length for RWM, pCN, Hamiltonian MCMC (left) and MALA and l-MwG (right). Bottom row: acceptance rate as a function of domain length (left) and mean squared error in posterior mean (right).

We solve the Gaussian inverse problem by RWM, MALA, pCN, Hamiltonian MCMC and l-MwG. The set-up and tuning of the algorithms are as described in Examples 1 and 2, and summarized in Table 1. The l-MwG sampler with covariance localization does not require localization since the prior covariance is banded (tridiagonal). The precision matrix on the other hand cannot be localized efficiently because the bandwidth of the prior precision matrix is large (see Figure 5.4), and also increases with  $n$ . We thus do *not* localize the l-MwG sampler in precision matrix implementation and condition on all variables during sampling, not only on nearby variables.

For each algorithm and dimension, we compute IACT (see Table 1 for the rates with which IACT increases with dimension for the various algorithms). We observe that IACT increases for all algorithms we consider, as illustrated by Figure 5.4. We observe that IACT for the l-MwG samplers now also increases. The rate is  $n^{1/2}$  which is larger than the rate of MALA which, as in examples 1 and 2, is equal to  $n^{1/4}$ . The increase in IACT with dimension can be understood within our theory by the increase in condition number with dimension. This numerical experiment thus suggests that our assumption of moderate condition number is indeed necessary (rather than being a tool for proving the theorems), which further corroborates our claim that l-MwG is effective (nearly dimension independent) for a unified class of problems with banded precision *and* covariance matrix. The bandedness of one implies bandedness of the other by the small condition number.

**6. Summary and conclusions.** We studied the Gibbs sampler for Gaussian distributions with banded covariance and precision matrices. We proved that the distribution of the samples converges geometrically fast to the Gaussian target distribution, and that the rate of convergence is independent of the dimension of the target Gaussian. The convergence rate, however, depends on the condition number of the covariance matrix, and convergence is fast

only if the condition number is small. If the covariance matrix is banded and the condition number is small, then the precision matrix is also banded. Thus, the Gibbs sampler is effective for a unified class of problems with banded precision and covariance matrices.

The Gibbs sampler is a building block of a localized Metropolis-within-Gibbs (l-MwG) sampler that can be used to solve Bayesian inverse problems. We argued that l-MwG can be expected to be effective if the Bayesian inverse problem is characterized by banded prior covariance and precision matrices and by local observations. If prior covariance and precision matrices are nearly banded, we propose to “localize” the problem by setting small off-diagonal elements equal to zero. The localization introduces a small error in the resulting posterior distribution. We can explicitly bound these errors and thus specify conditions where the errors are small. We also demonstrated our ideas by numerical examples, and illustrated the limitations of l-MwG by deliberately violating some of our assumptions.

The main goal of our study is to demonstrate that ideas of covariance localization in the ensemble Kalman filter (EnKF) have relevance in MCMC. Covariance localization is routinely used to make EnKF applicable to problems in numerical weather prediction where the dimension can exceed  $10^8$ , at the cost of a small bias. This bias arises from localizing the problem, i.e., restricting nonzero correlations to a specified neighborhood, and restricting the influence of an observation to its neighborhood. We showed that similar steps can be applied when solving a Gaussian inverse problem by MCMC. Inverse problems with nearly banded structure can be localized to have a banded structure, at the cost of a small bias, and banded problems can be solved efficiently by l-MwG.

Our study neglects many practical challenges; for example, localization may require some tuning, which in itself can be computationally expensive. More importantly, we have not rigorously defined localization for non-Gaussian problems, where enforcing bandedness of the covariance matrices may not be sufficient because higher moments become important. Taking inspiration instead from the sparsity of the precision matrix, a useful route may be to consider the conditional independence structure of more general non-Gaussian Markov random fields [48]. We hope to address these issues in future work.

**Appendix A. Convergence rates for Gibbs samplers.** In this section, we prove Theorems 2.1-2.4. Since the Gibbs sampler with block-size  $q$  is a generalization of the standard Gibbs sampler (with block size  $q = 1$ ), we only prove Theorems 2.2 and 2.4. Theorems 2.1 and 2.3 follow by setting  $q = 1$ .

**A.1. Review of Gibbs and Gauss-Seidel.** Our strategy for proving these theorems relies on the Gauss-Seidel operator associated with the Gibbs sampler. The connection between the Gibbs sampler and the Gauss-Seidel operator is well documented [19, 21, 46], but we briefly review it here so that our paper can be read and understood independently.

We consider sampling  $\mathbf{x} \sim \mathcal{N}(\mathbf{m}, \mathbf{\Omega}^{-1})$  using the Gibbs sampler of block size  $q$ , assuming  $\mathbf{\Omega}$  is of dimension  $mq \times mq$ . We will use  $\mathbf{\Omega}_{i,j}$  to denote its  $(i, j)$ - $q \times q$  sub-block, which should not be confused with the matrix entry  $[\mathbf{\Omega}]_{i,j}$ . We say an  $mq \times mq$  matrix  $\mathbf{\Omega}$  is block-strictly-lower-triangular (BSLT), if  $\mathbf{\Omega}_{i,j}$  is nonzero only if  $i > j$ . We define block-diagonal and block-strictly-upper-triangular (BSUT) in an analogous way. Let  $\mathbf{\Omega} = \mathbf{\Omega}_L + \mathbf{\Omega}_D + \mathbf{\Omega}_U$  be the BSLT + block-diagonal + BSUT decomposition of the precision matrix  $\mathbf{\Omega}$ . In other words,  $\mathbf{\Omega}_L$  consists of the blocks  $\{\mathbf{\Omega}_{i,j}\}_{i>j}$  of  $\mathbf{\Omega}$ ,  $\mathbf{\Omega}_D$  consists of the diagonal blocks of  $\mathbf{\Omega}$ , and

$$\boldsymbol{\Omega}_U = \boldsymbol{\Omega}_L^T.$$

We investigate how the  $j$ -th coordinate is updated at the  $k+1$ -th iteration. For simplicity, let us write the state before this coordinate update as

$$(\mathbf{z}_1, \dots, \mathbf{z}_m) = (\mathbf{x}_1^{k+1}, \dots, \mathbf{x}_{j-1}^{k+1}, \mathbf{x}_j^k, \dots, \mathbf{x}_m^k).$$

Then  $\log(p(\mathbf{z}))$ , ignoring a constant term, can be written as

$$\begin{aligned} -\frac{1}{2}(\mathbf{z} - \mathbf{m})^T \boldsymbol{\Omega} (\mathbf{z} - \mathbf{m}) &= -\frac{1}{2} \sum_{i,i'} (\mathbf{z}_i - \mathbf{m}_i)^T \boldsymbol{\Omega}_{i,i'} (\mathbf{z}_{i'} - \mathbf{m}_{i'}) \\ &= -\frac{1}{2} (\mathbf{z}_j - \mathbf{m}_j)^T \boldsymbol{\Omega}_{j,j} (\mathbf{z}_j - \mathbf{m}_j) - \frac{1}{2} (\mathbf{z}_j - \mathbf{m}_j)^T \sum_{i \neq j} \boldsymbol{\Omega}_{j,i} (\mathbf{z}_i - \mathbf{m}_i) \\ &\quad - \frac{1}{2} \sum_{i \neq j} (\mathbf{z}_i - \mathbf{m}_i)^T \boldsymbol{\Omega}_{i,j} (\mathbf{z}_j - \mathbf{m}_j) + F'_j(\mathbf{z}) \\ &= -\frac{1}{2} (\mathbf{z}_j - \mathbf{m}'_j)^T \boldsymbol{\Omega}_{j,j} (\mathbf{z}_j - \mathbf{m}'_j)^T + F_j(\mathbf{z}). \end{aligned}$$

Here  $F_j$  and  $F'_j$  are functions independent of  $\mathbf{z}_j$ , and

$$\mathbf{m}'_j := \mathbf{m}_j - \sum_{i \neq j} \boldsymbol{\Omega}_{j,j}^{-1} \boldsymbol{\Omega}_{j,i} (\mathbf{z}_i - \mathbf{m}_i) = \mathbf{m}_j - \sum_{i < j} \boldsymbol{\Omega}_{j,j}^{-1} \boldsymbol{\Omega}_{j,i} (\mathbf{x}_i^{k+1} - \mathbf{m}_i) - \sum_{i > j} \boldsymbol{\Omega}_{j,j}^{-1} \boldsymbol{\Omega}_{j,i} (\mathbf{x}_i^k - \mathbf{m}_i).$$

Using Bayes' formula, we find that the probability of  $\mathbf{x}_j^{k+1}$  conditioned on  $\mathbf{x}_i^{k+1}$ ,  $i < j$  and  $\mathbf{x}_i^k$ ,  $i > j$  is proportional to  $\exp(-\frac{1}{2}(\mathbf{z}_j - \mathbf{m}'_j)^T \boldsymbol{\Omega}_{j,j} (\mathbf{z}_j - \mathbf{m}'_j))$ . In other words, the updated coordinate has the distribution

$$(A.1) \quad \mathbf{x}_j^{k+1} \sim \mathcal{N} \left( \mathbf{m}_j - \sum_{i < j} \boldsymbol{\Omega}_{j,j}^{-1} \boldsymbol{\Omega}_{j,i} (\mathbf{x}_i^{k+1} - \mathbf{m}_i) - \sum_{i > j} \boldsymbol{\Omega}_{j,j}^{-1} \boldsymbol{\Omega}_{j,i} (\mathbf{x}_i^k - \mathbf{m}_i), \boldsymbol{\Omega}_{j,j}^{-1} \right).$$

One way to obtain a sample of this distribution is to find the solution,  $\mathbf{x}_j^{k+1}$ , of the linear equation

$$(A.2) \quad \boldsymbol{\Omega}_{j,j} (\mathbf{x}_j^{k+1} - \mathbf{m}_j) + \sum_{i < j} \boldsymbol{\Omega}_{j,i} (\mathbf{x}_i^{k+1} - \mathbf{m}_i) + \sum_{i > j} \boldsymbol{\Omega}_{j,i} (\mathbf{x}_i^k - \mathbf{m}_i) = \xi_j^{k+1}$$

where  $\xi_j^{k+1}$  is an independent sample from  $\mathcal{N}(0, \boldsymbol{\Omega}_{j,j})$ .

Let  $\boldsymbol{\Omega} = \boldsymbol{\Omega}_L + \boldsymbol{\Omega}_D + \boldsymbol{\Omega}_U$  be the BSLT + block-diagonal + BSUT decomposition of the precision matrix  $\boldsymbol{\Omega}$ . If we concatenate (A.2) for all coordinates  $j$ , the equation becomes

$$(\boldsymbol{\Omega}_L + \boldsymbol{\Omega}_D)(\mathbf{x}^{k+1} - \mathbf{m}) + \boldsymbol{\Omega}_U(\mathbf{x}^k - \mathbf{m}) = \boldsymbol{\xi}^{k+1},$$

where  $\boldsymbol{\xi}^{k+1}$  is the concatenation of  $\xi_j^{k+1}$ , and distributed as  $\boldsymbol{\xi}^{k+1} \sim \mathcal{N}(0, \boldsymbol{\Omega}_D)$ . An equivalent representation is

$$(A.3) \quad (\mathbf{x}^{k+1} - \mathbf{m}) = -(\boldsymbol{\Omega}_L + \boldsymbol{\Omega}_D)^{-1} \boldsymbol{\Omega}_U (\mathbf{x}^k - \mathbf{m}) + (\boldsymbol{\Omega}_L + \boldsymbol{\Omega}_D)^{-1} \boldsymbol{\xi}^{k+1}.$$

The correlation between two consecutive iterations then is determined by

$$\mathbf{G} := -(\boldsymbol{\Omega}_L + \boldsymbol{\Omega}_D)^{-1}\boldsymbol{\Omega}_U.$$

The spectral radius of  $\mathbf{G}$  decides how fast the Gibbs sampler converges in  $l_2$  norm.

The matrix  $\mathbf{G}$  is known as the ‘‘Gauss-Seidel operator’’, which is also used in the iterative solution of linear equations. Recall that  $\mathcal{N}(0, \mathbf{C})$  is the invariant distribution of  $\mathbf{x}^k - \mathbf{m}$ . By comparing covariances on both sides of (A.3), we find that

$$(A.4) \quad \mathbf{C} = \mathbf{G}\mathbf{C}\mathbf{G}^T + (\boldsymbol{\Omega}_L + \boldsymbol{\Omega}_D)^{-1}\boldsymbol{\Omega}_D(\boldsymbol{\Omega}_L + \boldsymbol{\Omega}_D)^{-T}.$$

It follows that  $\mathbf{C} \preceq \mathbf{G}\mathbf{C}\mathbf{G}^T$ , which in turn implies that the spectral radius of  $\mathbf{G}$  is less than 1, which implies convergence. Here and below, for two symmetric matrices  $\mathbf{A}$  and  $\mathbf{B}$ , we use  $\mathbf{A} \preceq \mathbf{B}$  to indicate that  $\mathbf{B} - \mathbf{A}$  is positive semidefinite. However, in order to show the convergence rate is dimension-independent, we need to exploit the banded structure of  $\mathbf{C}$  or  $\boldsymbol{\Omega}$ , which will be the purpose of the next section.

**A.2. Gauss-Seidel with localized structures.** First we need two estimates.

**Lemma A.1.** *For any positive definite  $qm \times qm$  matrix  $\mathbf{C}$ , denote its maximum eigenvalue as  $\lambda_{\max}$ , its minimum eigenvalue as  $\lambda_{\min}$ , its condition number as  $\mathcal{C} = \lambda_{\max}/\lambda_{\min}$ , its inverse  $\boldsymbol{\Omega} = \mathbf{C}^{-1}$ . Then the  $q \times q$  blocks satisfy:*

$$(A.5) \quad \lambda_{\min}\mathbf{I} \preceq \mathbf{C}_{i,i} \preceq \lambda_{\max}\mathbf{I}, \quad \lambda_{\max}^{-1}\mathbf{I} \preceq \boldsymbol{\Omega}_{i,i} \preceq \lambda_{\min}^{-1}\mathbf{I},$$

$$(A.6) \quad \|\boldsymbol{\Omega}_{i,i}^{-1/2}\boldsymbol{\Omega}_{i,j}\boldsymbol{\Omega}_{j,j}^{-1/2}\| \leq 1 - \mathcal{C}^{-1}, \quad \|\mathbf{C}_{i,i}^{-1/2}\mathbf{C}_{i,j}\mathbf{C}_{j,j}^{-1/2}\| \leq 1 - \mathcal{C}^{-1}.$$

*Proof.* Let  $\lambda_i$  be an eigenvalue of  $\mathbf{C}_{i,i}$  and  $v \in \mathbb{R}^q$  be one of its eigenvectors with norm 1. Let  $\mathbf{v}$  be the  $\mathbb{R}^{qm}$  vector with its  $i$ -th block being  $v$ . Then

$$\lambda_i = v^T \mathbf{C}_{i,i} v = \mathbf{v}^T \mathbf{C} \mathbf{v} \in [\lambda_{\min}, \lambda_{\max}].$$

The left inequality in (A.5) follows. The right inequality of equation (A.5) can be derived in a similar fashion.

Let  $\mathbf{x}$  and  $\mathbf{y}$  be the left and right singular vectors corresponding to the largest singular value of  $\Gamma_{i,j} = \boldsymbol{\Omega}_{i,i}^{-1/2}\boldsymbol{\Omega}_{i,j}\boldsymbol{\Omega}_{j,j}^{-1/2}$ . The vectors  $\mathbf{x}$  and  $\mathbf{y}$  are of dimension  $q$ , have norm one,  $\|\mathbf{x}\|_2 = \|\mathbf{y}\|_2 = 1$ , and  $\mathbf{x}^T \Gamma_{i,j} \mathbf{y} = \|\Gamma_{i,j}\|$ . Now consider an  $qm$  dimensional vector  $\mathbf{v}$ , where its  $i$ -th block is  $\boldsymbol{\Omega}_{i,i}^{-1/2}\mathbf{x}$ , its  $j$ -th block is  $-\boldsymbol{\Omega}_{j,j}^{-1/2}\mathbf{y}$ , and all other blocks are zero. Then

$$\begin{aligned} \mathbf{v}^T \boldsymbol{\Omega} \mathbf{v} &= \mathbf{x}^T \boldsymbol{\Omega}_{i,i}^{-1/2} \boldsymbol{\Omega}_{i,i} \boldsymbol{\Omega}_{i,i}^{-1/2} \mathbf{x} - 2\mathbf{x}^T \boldsymbol{\Omega}_{i,i}^{-1/2} \boldsymbol{\Omega}_{i,j} \boldsymbol{\Omega}_{j,j}^{-1/2} \mathbf{y} + \mathbf{y}^T \boldsymbol{\Omega}_{j,j}^{-1/2} \boldsymbol{\Omega}_{j,j} \boldsymbol{\Omega}_{j,j}^{-1/2} \mathbf{y} \\ &= 2 - 2\mathbf{x}^T \Gamma_{i,j} \mathbf{y} = 2(1 - \|\Gamma_{i,j}\|). \end{aligned}$$

On the other hand,

$$\|\mathbf{v}\|^2 = \|\boldsymbol{\Omega}_{i,i}^{-1/2}\mathbf{x}\|^2 + \|\boldsymbol{\Omega}_{j,j}^{-1/2}\mathbf{y}\|^2 \geq 2\lambda_{\min}.$$

Thus

$$2(1 - \|\Gamma_{i,j}\|) = 2\mathbf{v}^T \boldsymbol{\Omega} \mathbf{v} \geq 2\lambda_{\min} \lambda_{\max}^{-1} = 2\mathcal{C}^{-1}.$$

The left inequality in (A.6) follows. Since the derivation above uses nothing of  $\boldsymbol{\Omega}$  other than its eigenvalues, so the right inequality in (A.6) also holds.  $\blacksquare$

For our proofs below, we need the following bound for an operator norm. For  $q = 1$ , this bound appeared in [7] as inequality (A2). Note that this bound is well-suited for block-sparse  $\mathbf{A}$  since then the right hand side consists of only a few terms.

**Lemma A.2.** *For any  $qm \times qm$  matrix  $\mathbf{A}$ , the following holds*

$$\|\mathbf{A}\| \leq \left( \max_{i=1, \dots, m} \sum_{j=1}^m \|\mathbf{A}_{i,j}\| \right)^{1/2} \left( \max_{i=1, \dots, m} \sum_{j=1}^m \|\mathbf{A}_{j,i}\| \right)^{1/2}.$$

*Proof.* First we show the claim for symmetric  $\mathbf{A} = \mathbf{A}^T$ . In this case, the bound for the norm of  $\mathbf{A}$  is

$$(A.7) \quad \|\mathbf{A}\| \leq \max_{i=1, \dots, m} \sum_{j=1}^m \|\mathbf{A}_{i,j}\|.$$

Let  $\mathbf{v} = [\mathbf{v}_1, \dots, \mathbf{v}_m] \in \mathbb{R}^{qm}$  be an eigenvector so that  $\lambda \mathbf{v} = \mathbf{A} \mathbf{v}$  while  $|\lambda| = \|\mathbf{A}\|$ . Suppose  $\|\mathbf{v}_{i_*}\| = \max_i \{\|\mathbf{v}_i\|\}$ , then

$$|\lambda| \|\mathbf{v}_{i_*}\| = \|\lambda \mathbf{v}_{i_*}\| = \left\| \sum_{j=1}^m \mathbf{A}_{i_*,j} \mathbf{v}_j \right\| \leq \sum_{j=1}^m \|\mathbf{A}_{i_*,j}\| \|\mathbf{v}_j\| \leq \|\mathbf{v}_{i_*}\| \sum_{j=1}^m \|\mathbf{A}_{i_*,j}\|.$$

This leads to  $\|\mathbf{A}\| \leq \sum_{j=1}^m \|\mathbf{A}_{i_*,j}\|$  and hence (A.7).

For a general  $\mathbf{A}$ , note that  $\|\mathbf{A}\| = \|\mathbf{A}^T \mathbf{A}\|^{1/2}$ . The matrix  $\mathbf{P} = \mathbf{A}^T \mathbf{A}$  is symmetric, and its blocks are

$$\mathbf{P}_{i,j} = \sum_k \mathbf{A}_{k,i}^T \mathbf{A}_{k,j}.$$

Applying (A.7) to  $\mathbf{P}$ , we obtain

$$\begin{aligned} \|\mathbf{P}\| &\leq \max_i \sum_{j=1}^m \|\mathbf{P}_{i,j}\| \leq \max_i \sum_j \sum_k \|\mathbf{A}_{k,i}^T \mathbf{A}_{k,j}\| \\ &\leq \max_i \sum_k \sum_j \|\mathbf{A}_{k,i}\| \|\mathbf{A}_{k,j}\| \\ &\leq \max_i \sum_k \|\mathbf{A}_{k,i}\| \sum_j \|\mathbf{A}_{k,j}\| \\ &\leq \left( \max_i \sum_k \|\mathbf{A}_{k,i}\| \right) \left( \max_i \sum_j \|\mathbf{A}_{i,j}\| \right). \end{aligned}$$

This leads to our general claim. ■

Now we are at the position to establish bounds for the Gauss Seidel operator.

**Lemma A.3.** *If  $\mathbf{\Omega}$  is block-tridiagonal with  $\mathcal{C}$  being its condition number, then*

$$\mathbf{GCG}^T \preceq \frac{\mathcal{C}(1 - \mathcal{C}^{-1})^2}{1 + \mathcal{C}(1 - \mathcal{C}^{-1})^2} \mathbf{C}.$$



*Proof.* Since  $\mathbf{\Omega}$  is block-tridiagonal,  $\mathbf{\Omega}_U$  has at most one nonzero block in each row and each column, and, likewise,  $\mathbf{\Omega}_D^{-1/2}\mathbf{\Omega}_U\mathbf{\Omega}_D^{-1/2}$  has at most one nonzero block in each row and each column. Therefore, by Lemma A.2

$$\left\| \mathbf{\Omega}_D^{-1/2}\mathbf{\Omega}_U\mathbf{\Omega}_D^{-1/2} \right\| \leq \max_{i=1,\dots,m-1} \left\| \mathbf{\Omega}_{i,i}^{-1/2}\mathbf{\Omega}_{i,i+1}\mathbf{\Omega}_{i+1,i+1}^{-1/2} \right\|,$$

which by Lemma A.1 is bounded by  $1 - \mathcal{C}^{-1}$ .

To continue, we look at the right hand side of (A.4). We want to show that for some  $\gamma > 0$ ,

$$(A.8) \quad \mathbf{GCG}^T \preceq \gamma(\mathbf{\Omega}_L + \mathbf{\Omega}_D)^{-1}\mathbf{\Omega}_D(\mathbf{\Omega}_L + \mathbf{\Omega}_D)^{-T}$$

For this purpose, note that

$$\mathbf{GCG}^T = (\mathbf{\Omega}_L + \mathbf{\Omega}_D)^{-1}\mathbf{\Omega}_U\mathbf{C}\mathbf{\Omega}_U^T(\mathbf{\Omega}_L + \mathbf{\Omega}_D)^{-T},$$

and that

$$\mathbf{\Omega}_U\mathbf{C}\mathbf{\Omega}_U^T = \mathbf{\Omega}_D^{1/2}(\mathbf{\Omega}_D^{-1/2}\mathbf{\Omega}_U\mathbf{\Omega}_D^{-1/2})(\mathbf{\Omega}_D^{1/2}\mathbf{C}\mathbf{\Omega}_D^{1/2})(\mathbf{\Omega}_D^{-1/2}\mathbf{\Omega}_U\mathbf{\Omega}_D^{-1/2})^T\mathbf{\Omega}_D^{1/2}.$$

Thus, in order to prove (A.8), it suffices to find a  $\gamma$  such that

$$\left\| (\mathbf{\Omega}_D^{-1/2}\mathbf{\Omega}_U\mathbf{\Omega}_D^{-1/2})(\mathbf{\Omega}_D^{1/2}\mathbf{C}\mathbf{\Omega}_D^{1/2})(\mathbf{\Omega}_D^{-1/2}\mathbf{\Omega}_U\mathbf{\Omega}_D^{-1/2})^T \right\| \leq \gamma.$$

By Lemma A.1, this is straight forward, since we have that

$$\begin{aligned} & \left\| (\mathbf{\Omega}_D^{-1/2}\mathbf{\Omega}_U\mathbf{\Omega}_D^{-1/2})(\mathbf{\Omega}_D^{1/2}\mathbf{C}\mathbf{\Omega}_D^{1/2})(\mathbf{\Omega}_D^{-1/2}\mathbf{\Omega}_U\mathbf{\Omega}_D^{-1/2})^T \right\| \\ & \leq (1 - \mathcal{C}^{-1})^2 \|\mathbf{\Omega}_D\| \|\mathbf{C}\| \leq \mathcal{C}(1 - \mathcal{C}^{-1})^2 =: \gamma, \end{aligned}$$

since  $\mathbf{\Omega}_D$  is diagonal with blocks bounded in operator norm by  $\lambda_{\min}^{-1}$ .

Finally, we can plug (A.8) into (A.4), and find that

$$\mathbf{C} = \mathbf{GCG}^T + (\mathbf{\Omega}_L + \mathbf{\Omega}_D)^{-1}\mathbf{\Omega}_D(\mathbf{\Omega}_L + \mathbf{\Omega}_D)^{-T} \succeq (\gamma^{-1} + 1)\mathbf{GCG}^T. \quad \blacksquare$$

**Lemma A.4.** *If  $\mathbf{C}$  is block-tridiagonal with  $\mathcal{C}$  being its condition number, then*

$$\mathbf{GCG}^T \preceq \frac{2(1 - \mathcal{C}^{-1})^2\mathcal{C}^4}{1 + 2(1 - \mathcal{C}^{-1})^2\mathcal{C}^4}\mathbf{C}.$$

*Proof.* Since  $\mathbf{\Omega}^{-1} = \mathbf{C}$ , we apply the Woodbury's formula to  $(\mathbf{\Omega}_L + \mathbf{\Omega}_D)^{-1} = (\mathbf{\Omega} - \mathbf{\Omega}_U)^{-1}$ ,

$$(\mathbf{\Omega}_L + \mathbf{\Omega}_D)^{-1} = (\mathbf{\Omega} - \mathbf{\Omega}_U)^{-1} = \mathbf{C} + \mathbf{C}\mathbf{\Omega}_U(\mathbf{I} - \mathbf{C}\mathbf{\Omega}_U)^{-1}\mathbf{C} = (\mathbf{I} - \mathbf{C}\mathbf{\Omega}_U)^{-1}\mathbf{C}.$$

Consequentially,  $\mathbf{G} = (\mathbf{I} - \mathbf{C}\mathbf{\Omega}_U)^{-1}\mathbf{C}\mathbf{\Omega}_U$ .

Next, we claim that  $\mathbf{C}\boldsymbol{\Omega}_U$  is BUT, and that only the blocks  $(\mathbf{C}\boldsymbol{\Omega}_U)_{i,i}, (\mathbf{C}\boldsymbol{\Omega}_U)_{i,i+1}$  are nonzero. To see it is BUT, recall that  $\mathbf{C}$  is block-tridiagonal,  $(\boldsymbol{\Omega}_U)_{i,j} = \boldsymbol{\Omega}_{i,j}\mathbf{1}_{i \leq j-1}$ ,

$$(\mathbf{C}\boldsymbol{\Omega}_U)_{i,j} = \mathbf{C}_{i,i-1}\boldsymbol{\Omega}_{i-1,j}\mathbf{1}_{i \leq j} + \mathbf{C}_{i,i}\boldsymbol{\Omega}_{i,j}\mathbf{1}_{i \leq j-1} + \mathbf{C}_{i,i+1}\boldsymbol{\Omega}_{i+1,j}\mathbf{1}_{i \leq j-2}.$$

Thus  $(\mathbf{C}\boldsymbol{\Omega}_U)_{i,j}$  is nonzero only if  $i \leq j$ , i.e.,  $\mathbf{C}\boldsymbol{\Omega}_U$  is BUT. Moreover, if  $j \geq i+2$ , by the identity  $\mathbf{C}\boldsymbol{\Omega} = \mathbf{I}$ , we have

$$\mathbf{0} = (\mathbf{C}\boldsymbol{\Omega})_{i,j} = \mathbf{C}_{i,i-1}\boldsymbol{\Omega}_{i-1,j} + \mathbf{C}_{i,i}\boldsymbol{\Omega}_{i,j} + \mathbf{C}_{i,i+1}\boldsymbol{\Omega}_{i+1,j} = (\mathbf{C}\boldsymbol{\Omega}_U)_{i,j},$$

proving our claim.

Next, note that for  $j = i$ , we have

$$(\mathbf{C}\boldsymbol{\Omega}_U)_{i,i} = \mathbf{C}_{i,i-1}\boldsymbol{\Omega}_{i-1,i}\mathbf{1}_{i \leq i} + \mathbf{C}_{i,i}\boldsymbol{\Omega}_{i,i}\mathbf{1}_{i \leq i-1} + \mathbf{C}_{i,i+1}\boldsymbol{\Omega}_{i+1,i}\mathbf{1}_{i \leq i-2} = \mathbf{C}_{i,i-1}\boldsymbol{\Omega}_{i-1,i}.$$

Likewise, for  $j = i+1$ , we have

$$\mathbf{0} = (\mathbf{C}\boldsymbol{\Omega})_{i,i+1} = \mathbf{C}_{i,i-1}\boldsymbol{\Omega}_{i-1,i+1} + \mathbf{C}_{i,i}\boldsymbol{\Omega}_{i,i+1} + \mathbf{C}_{i,i+1}\boldsymbol{\Omega}_{i+1,i+1} = (\mathbf{C}\boldsymbol{\Omega}_U)_{i,i+1} + \mathbf{C}_{i,i+1}\boldsymbol{\Omega}_{i+1,i+1}.$$

In other words,  $(\mathbf{C}\boldsymbol{\Omega}_U)_{i,i+1} = -\mathbf{C}_{i,i+1}\boldsymbol{\Omega}_{i+1,i+1}$ .

Applying Lemma A.2 leads to

$$\|\mathbf{C}\boldsymbol{\Omega}_U\| \leq \left( \max_{i=1, \dots, m} \{ \|(\mathbf{C}\boldsymbol{\Omega}_U)_{i,i}\| + \|(\mathbf{C}\boldsymbol{\Omega}_U)_{i,i+1}\| \} \right)^{1/2} \left( \max_{i=1, \dots, m} \|(\mathbf{C}\boldsymbol{\Omega}_U)_{i,i}\| \right)^{1/2}.$$

Applying Lemma A.1 to  $(\mathbf{C}\boldsymbol{\Omega}_U)_{i,i} = \mathbf{C}_{i,i-1}\boldsymbol{\Omega}_{i-1,i}$  gives

$$\begin{aligned} \|(\mathbf{C}\boldsymbol{\Omega}_U)_{i,i}\| &\leq \|\mathbf{C}_{i,i}^{1/2}\| \|\mathbf{C}_{i,i}^{-1/2}\mathbf{C}_{i,i-1}\mathbf{C}_{i-1,i-1}^{-1/2}\| \|\mathbf{C}_{i-1,i-1}^{1/2}\| \|\boldsymbol{\Omega}_{i-1,i-1}^{1/2}\| \|\boldsymbol{\Omega}_{i-1,i-1}^{-1/2}\boldsymbol{\Omega}_{i-1,i}\boldsymbol{\Omega}_{i,i}^{-1/2}\| \|\boldsymbol{\Omega}_{i,i}^{1/2}\| \\ &\leq (1 - \mathcal{C}^{-1})^2 \mathcal{C} \leq (1 - \mathcal{C}^{-1})\mathcal{C}. \end{aligned}$$

Similarly,  $(\mathbf{C}\boldsymbol{\Omega}_U)_{i,i+1} = -\mathbf{C}_{i,i+1}\boldsymbol{\Omega}_{i+1,i+1}$ , which by Lemma A.1 implies that

$$\|(\mathbf{C}\boldsymbol{\Omega}_U)_{i,i+1}\| \leq \|\mathbf{C}_{i,i}^{1/2}\| \|\mathbf{C}_{i,i}^{-1/2}\mathbf{C}_{i,i+1}\mathbf{C}_{i+1,i+1}^{-1/2}\| \|\mathbf{C}_{i+1,i+1}^{1/2}\| \|\boldsymbol{\Omega}_{i+1,i+1}\| \leq (1 - \mathcal{C}^{-1})\mathcal{C}.$$

Consequently, another application of Lemma A.2 implies that

$$\|\mathbf{C}\boldsymbol{\Omega}_U\| \leq \sqrt{2}(1 - \mathcal{C}^{-1})\mathcal{C}.$$

To continue, we again want to use (A.4) by exploiting relations like (A.8). We first note that

$$\begin{aligned} \mathbf{G}\mathbf{C}\mathbf{G}^T &= (\mathbf{I} - \mathbf{C}\boldsymbol{\Omega}_U)^{-1}\mathbf{C}\boldsymbol{\Omega}_U\mathbf{C}\boldsymbol{\Omega}_U^T\mathbf{C}(\mathbf{I} - \mathbf{C}\boldsymbol{\Omega}_U)^{-T}, \\ (\boldsymbol{\Omega}_L + \boldsymbol{\Omega}_D)^{-1}\boldsymbol{\Omega}_D(\boldsymbol{\Omega}_L + \boldsymbol{\Omega}_D)^{-T} &= (\mathbf{I} - \mathbf{C}\boldsymbol{\Omega}_U)^{-1}\mathbf{C}\boldsymbol{\Omega}_D\mathbf{C}(\mathbf{I} - \mathbf{C}\boldsymbol{\Omega}_U)^{-T}. \end{aligned}$$

Using  $\|\mathbf{C}\boldsymbol{\Omega}_U\| \leq \sqrt{2}(1 - \mathcal{C}^{-1})\mathcal{C}$ , we have

$$\mathbf{C}\boldsymbol{\Omega}_U\mathbf{C}\boldsymbol{\Omega}_U^T\mathbf{C} \preceq 2(1 - \mathcal{C}^{-1})^2\mathcal{C}^2\lambda_{\max}\mathbf{I}.$$

Moreover,

$$\mathbf{C}\boldsymbol{\Omega}_D\mathbf{C} \succeq \lambda_{\max}^{-1}\mathbf{C}\mathbf{C}\mathbf{I} \succeq \lambda_{\max}^{-1}\lambda_{\min}^2\mathbf{I}.$$

Consequently,  $\mathbf{C}\boldsymbol{\Omega}_U\mathbf{C}\boldsymbol{\Omega}_U^T\mathbf{C} \preceq 2(1 - \mathcal{C}^{-1})^2\mathcal{C}^4\mathbf{C}\boldsymbol{\Omega}_D\mathbf{C}$  and

$$\mathbf{G}\mathbf{C}\mathbf{G}^T \preceq 2(1 - \mathcal{C}^{-1})^2\mathcal{C}^4(\boldsymbol{\Omega}_L + \boldsymbol{\Omega}_D)^{-1}\boldsymbol{\Omega}_D(\boldsymbol{\Omega}_L + \boldsymbol{\Omega}_D)^{-T}.$$

Combining the above inequality with (A.4) leads to

$$\mathbf{C} = \mathbf{G}\mathbf{C}\mathbf{G}^T + (\boldsymbol{\Omega}_L + \boldsymbol{\Omega}_D)^{-1}\boldsymbol{\Omega}_D(\boldsymbol{\Omega}_L + \boldsymbol{\Omega}_D)^{-T} \succeq ((2(1 - \mathcal{C}^{-1})^2\mathcal{C}^4)^{-1} + 1)\mathbf{G}\mathbf{C}\mathbf{G}^T. \quad \blacksquare$$

**A.3. Proofs of the main theorems.** Armed with these results, the proofs for the main theorems follow from an elementary coupling argument.

*Proof of Theorems 2.2 and 2.4.* As discussed above, and illustrated in Section A.1, we can generate iterates from the Gibbs sampler with block-size  $q$  by solving the linear equations

$$(\mathbf{x}^{k+1} - \mathbf{m}) = \mathbf{G}(\mathbf{x}^k - \mathbf{m}) + (\boldsymbol{\Omega}_L + \boldsymbol{\Omega}_D)^{-1}\boldsymbol{\xi}^{k+1} \quad k = 0, 1, \dots,$$

where  $\boldsymbol{\xi}^{k+1}$  are i.i.d. samples from  $\mathcal{N}(0, \boldsymbol{\Omega}_D)$ .

Next we consider a random sample  $\mathbf{z}^0$  from  $\mathcal{N}(\mathbf{m}, \mathbf{C})$ . We can apply the block-Gibbs sampler with  $\mathbf{z}^0$  as the initial condition, while using the same sequence  $\boldsymbol{\xi}^k$ . In other words, we generate  $\mathbf{z}^{k+1}$  by letting

$$(\mathbf{z}^{k+1} - \mathbf{m}) = \mathbf{G}(\mathbf{z}^k - \mathbf{m}) + (\boldsymbol{\Omega}_L + \boldsymbol{\Omega}_D)^{-1}\boldsymbol{\xi}^{k+1} \quad k = 0, 1, \dots.$$

Since  $\mathcal{N}(\mathbf{m}, \mathbf{C})$  is the invariant measure for the Gibbs sampler, marginally  $\mathbf{z}^k \sim \mathcal{N}(\mathbf{m}, \mathbf{C})$ .

Next we look at the difference between the two Gibbs samplers,  $\Delta^k = \mathbf{x}^k - \mathbf{z}^k$ . Note that

$$\Delta^0 \sim \mathcal{N}(\mathbf{x}^0 - \mathbf{m}, \mathbf{C}), \quad \Delta^{k+1} = \mathbf{G}\Delta^k, \quad k = 0, 1, \dots.$$

Consequently,  $\Delta^k \sim \mathcal{N}(\mathbf{G}^k\Delta_0, \mathbf{G}^k\mathbf{C}(\mathbf{G}^T)^k)$ , where  $\Delta_0 := \mathbf{x}^0 - \mathbf{m}$ . Since

$$\Delta^0\Delta^{0T} = \mathbf{C}^{1/2}(\mathbf{C}^{-1/2}\Delta_0)(\mathbf{C}^{-1/2}\Delta_0)^T\mathbf{C}^{1/2} \preceq \|\mathbf{C}^{-1/2}\Delta_0\|^2\mathbf{C},$$

we find that

$$\begin{aligned} \mathbb{E}\|\mathbf{C}^{-1/2}\Delta^k\|^2 &= \|\mathbf{C}^{-1/2}\mathbf{G}^k\Delta_0\|^2 + \text{tr}(\mathbf{C}^{-1/2}\mathbf{G}^k\mathbf{C}(\mathbf{G}^T)^k\mathbf{C}^{-1/2}) \\ &= \text{tr}(\mathbf{C}^{-1/2}\mathbf{G}^k\Delta_0\Delta_0^T(\mathbf{G}^T)^k\mathbf{C}^{-1/2} + \mathbf{C}^{-1/2}\mathbf{G}^k\mathbf{C}(\mathbf{G}^T)^k\mathbf{C}^{-1/2}) \\ \text{(A.9)} \quad &\leq (1 + \|\mathbf{C}^{-1/2}\Delta_0\|^2) \cdot \text{tr}(\mathbf{C}^{-1/2}\mathbf{G}^k\mathbf{C}(\mathbf{G}^T)^k\mathbf{C}^{-1/2}). \end{aligned}$$

If  $\boldsymbol{\Omega}$  is block-tridiagonal, then, by Lemma A.3,

$$\mathbf{C}^{-1/2}\mathbf{G}^k\mathbf{C}(\mathbf{G}^T)^k\mathbf{C}^{-1/2} \leq \beta^k\mathbf{I}, \quad \beta = \frac{\mathcal{C}(1 - \mathcal{C}^{-1})^2}{1 + \mathcal{C}(1 - \mathcal{C}^{-1})^2}.$$

Combining the above inequality with (A.9) proves Theorem 2.4.

If  $\mathbf{C}$  is block-tridiagonal, then, by Lemma A.4,

$$\mathbf{C}^{-1/2}\mathbf{G}^k\mathbf{C}(\mathbf{G}^T)^k\mathbf{C}^{-1/2} \leq \beta^k\mathbf{I}, \quad \beta = \frac{2(1 - \mathcal{C}^{-1})^2\mathcal{C}^4}{1 + 2(1 - \mathcal{C}^{-1})^2\mathcal{C}^4}.$$

Combining the above inequality with (A.9) proves Theorem 2.2. \blacksquare

**Appendix B. Bias caused by localization.** In sections 3.1 and 3.2, we propose to localize the prior covariance or precision matrix, and apply the l-MwG. This leads to samples from the localized posterior distribution, not from the exact posterior distribution. In this section we show that the difference between these two distributions can be small.

First we need the following estimate.

**Lemma B.1.** *Suppose  $\mathbf{A}$  is a symmetric positive definite matrix, and  $\mathbf{B}$  is a symmetric matrix such that  $\|\mathbf{B}\| \leq \|\mathbf{A}^{-1}\|^{-1}$ , then*

$$\|(\mathbf{A} + \mathbf{B})^{-1} - \mathbf{A}^{-1}\| \leq \frac{\|\mathbf{A}^{-1}\|^2 \|\mathbf{B}\|}{1 - \|\mathbf{B}\| \|\mathbf{A}^{-1}\|}.$$

*Proof.* Let  $\mathbf{B} = \Psi L \Psi^T$  be the eigenvalue decomposition of matrix  $\mathbf{B}$ . Remove columns of  $\Psi$  that are eigenvectors of value 0, so  $L$  only contains nonsingular terms. Then by the Woodbury matrix identity

$$\mathbf{A}^{-1} - (\mathbf{A} + \Psi L \Psi^T)^{-1} = \mathbf{A}^{-1} \Psi (L^{-1} + \Psi^T \mathbf{A}^{-1} \Psi)^{-1} \Psi^T \mathbf{A}^{-1}.$$

Let  $v$  be the eigenvector corresponds to the largest absolute eigenvalue of  $(L^{-1} + \Psi^T \mathbf{A}^{-1} \Psi)^{-1}$ . Then

$$|v^T (L^{-1} + \Psi^T \mathbf{A}^{-1} \Psi) v| \geq |v^T L^{-1} v| - |v^T \Psi^T \mathbf{A}^{-1} \Psi v| \geq \|L\|^{-1} - \|\mathbf{A}^{-1}\|.$$

Moreover,  $\|L\| = \|\mathbf{B}\|$ , so  $\|(L^{-1} + \Psi^T \mathbf{A}^{-1} \Psi)^{-1}\| \leq (\|\mathbf{B}\|^{-1} - \|\mathbf{A}^{-1}\|)^{-1}$ , and

$$\|(\mathbf{A} + \mathbf{B})^{-1} - \mathbf{A}^{-1}\| \leq \frac{\|\mathbf{A}^{-1}\|^2}{\|\mathbf{B}\|^{-1} - \|\mathbf{A}^{-1}\|}. \quad \blacksquare$$

**Proposition B.2.** *Let  $\mathbf{C}$  be a prior covariance matrix and  $\mathbf{H}$  be an observation matrix. Let  $\mathbf{C}_{\text{loc}}$  and  $\mathbf{H}_{\text{loc}}$  be localized covariance and observation matrices, and let  $\delta_C$  and  $\delta_H$  be as defined in (3.2) and (3.4).*

a) *The localized prior covariance and observation matrices are small perturbations of the unlocalized covariance and observation matrices in the sense that*

$$\|\mathbf{C} - \mathbf{C}_{\text{loc}}\| \leq \delta_C, \quad \|\mathbf{H}_{\text{loc}} - \mathbf{H}\| \leq \delta_H.$$

*Moreover, if  $\delta_C \leq \|\mathbf{C}^{-1}\|^{-1}$ , then  $\mathbf{C}_{\text{loc}}$  is positive semidefinite.*

b) *If  $\delta_C \leq \|\mathbf{C}^{-1}\|^{-1}$ ,  $\Delta_1 \leq \|\widehat{\mathbf{C}}\|^{-1}$ , the localization creates a small perturbation of the posterior covariance matrix in the sense that*

$$\|\widehat{\mathbf{C}} - \widehat{\mathbf{C}}_{\text{loc}}\| \leq \frac{\|\widehat{\mathbf{C}}\|^2 \Delta_1}{1 - \Delta_1 \|\widehat{\mathbf{C}}\|}, \quad \Delta_1 := \frac{\|\mathbf{C}^{-1}\|^2 \delta_C}{1 - \delta_C \|\mathbf{C}^{-1}\|} + (2\delta_H + \delta_H^2) \|\mathbf{R}^{-1}\|.$$

c) *Under the same conditions as in b), the localization creates a small perturbation of the posterior mean in the sense that*

$$\begin{aligned} \|\widehat{\mathbf{m}}_{\text{loc}} - \widehat{\mathbf{m}}\| &\leq \left( \frac{\|\mathbf{C}^{-1}\|^2 \|\widehat{\mathbf{C}}\| \delta_C}{(1 - \delta_C \|\mathbf{C}^{-1}\|)(1 - \Delta_1 \|\widehat{\mathbf{C}}\|)} + \frac{\|\mathbf{C}^{-1}\| \|\widehat{\mathbf{C}}\|^2 \Delta_1}{1 - \Delta_1 \|\widehat{\mathbf{C}}\|} \right) \|\mathbf{m}\| \\ &\quad + \frac{\|\widehat{\mathbf{C}}\| \|\mathbf{R}^{-1}\|}{1 - \Delta_1 \|\widehat{\mathbf{C}}\|} (\|\widehat{\mathbf{C}}\| \Delta_1 + \delta_H) \|\mathbf{y}\|. \end{aligned}$$

*Proof.* For claim a), Define  $\Delta = \mathbf{C} - \mathbf{C}_{\text{loc}}$ , apply Lemma A.2 with block size 1,

$$\|\mathbf{C} - \mathbf{C}_{\text{loc}}\| \leq \left( \max_i \sum_j |[\Delta]_{i,j}| \right) = \delta_C.$$

The bound  $\|\mathbf{H} - \mathbf{H}_{\text{loc}}\| \leq \delta_H$  follows the same argument.

For claim b), we will exploit the identity  $\widehat{\mathbf{C}}^{-1} = \mathbf{C}^{-1} + \mathbf{H}^T \mathbf{R}^{-1} \mathbf{H}$ . By Lemma B.1,

$$\|\mathbf{C}^{-1} - \mathbf{C}_{\text{loc}}^{-1}\| \leq \frac{\|\mathbf{C}^{-1}\|^2 \delta_C}{1 - \delta_C \|\mathbf{C}^{-1}\|}.$$

Under our normalization assumption that  $\|\mathbf{H}\| = 1$ ,

$$\begin{aligned} \|\mathbf{H}^T \mathbf{R}^{-1} \mathbf{H} - \mathbf{H}_{\text{loc}}^T \mathbf{R}^{-1} \mathbf{H}_{\text{loc}}\| &\leq \|(\mathbf{H}^T - \mathbf{H}_{\text{loc}}^T) \mathbf{R}^{-1} \mathbf{H}\| + \|\mathbf{H}^T \mathbf{R}^{-1} (\mathbf{H} - \mathbf{H}_{\text{loc}})\| \\ &\quad + \|(\mathbf{H}^T - \mathbf{H}_{\text{loc}}^T) \mathbf{R}^{-1} (\mathbf{H} - \mathbf{H}_{\text{loc}})\| \\ \text{(B.1)} \qquad \qquad \qquad &\leq 2\delta_H \|\mathbf{R}^{-1} \mathbf{H}\| + \delta_H^2 \|\mathbf{R}^{-1}\| \leq (2\delta_H + \delta_H^2) \|\mathbf{R}^{-1}\|. \end{aligned}$$

Therefore

$$\|(\mathbf{C}^{-1} + \mathbf{H}^T \mathbf{R}^{-1} \mathbf{H}) - (\mathbf{C}_{\text{loc}}^{-1} + \mathbf{H}_{\text{loc}}^T \mathbf{R}^{-1} \mathbf{H}_{\text{loc}})\| \leq \frac{\|\mathbf{C}^{-1}\|^2 \delta_C}{1 - \delta_C \|\mathbf{C}^{-1}\|} + (2\delta_H + \delta_H^2) \|\mathbf{R}^{-1}\| =: \Delta_1.$$

We apply Lemma B.1 to  $\widehat{\mathbf{C}} = (\mathbf{C}^{-1} + \mathbf{H}^T \mathbf{R}^{-1} \mathbf{H})^{-1}$ , and obtain

$$\|\widehat{\mathbf{C}} - \widehat{\mathbf{C}}_{\text{loc}}\| \leq \frac{\|\widehat{\mathbf{C}}\|^2 \Delta_1}{1 - \Delta_1 \|\widehat{\mathbf{C}}\|}.$$

As a consequence, we also have that  $\|\widehat{\mathbf{C}}_{\text{loc}}\| \leq \frac{\|\widehat{\mathbf{C}}\|^2 \Delta_1}{1 - \Delta_1 \|\widehat{\mathbf{C}}\|} + \|\widehat{\mathbf{C}}\| = \frac{\|\widehat{\mathbf{C}}\|}{1 - \Delta_1 \|\widehat{\mathbf{C}}\|}$ .

As for claim c), the difference is given by

$$\widehat{\mathbf{m}}_{\text{loc}} - \widehat{\mathbf{m}} = (\widehat{\mathbf{C}}_{\text{loc}} \mathbf{C}_{\text{loc}}^{-1} - \widehat{\mathbf{C}} \mathbf{C}^{-1}) \mathbf{m} + (\widehat{\mathbf{C}}_{\text{loc}} \mathbf{H}_{\text{loc}}^T - \widehat{\mathbf{C}} \mathbf{H}^T) \mathbf{R}^{-1} \mathbf{y}.$$

The norm of the matrix  $(\widehat{\mathbf{C}}_{\text{loc}} \mathbf{H}_{\text{loc}}^T - \widehat{\mathbf{C}} \mathbf{H}^T) \mathbf{R}^{-1}$  can be bounded using claim b)

$$\begin{aligned} \|(\widehat{\mathbf{C}}_{\text{loc}} \mathbf{H}_{\text{loc}}^T - \widehat{\mathbf{C}} \mathbf{H}^T) \mathbf{R}^{-1}\| &\leq \|\widehat{\mathbf{C}} - \widehat{\mathbf{C}}_{\text{loc}}\| \|\mathbf{H}^T \mathbf{R}^{-1}\| + \|\widehat{\mathbf{C}}_{\text{loc}}\| \|\mathbf{H}_{\text{loc}} - \mathbf{H}\| \|\mathbf{R}^{-1}\| \\ &\leq \frac{\|\widehat{\mathbf{C}}\| \|\mathbf{R}^{-1}\|}{1 - \Delta_1 \|\widehat{\mathbf{C}}\|} (\|\widehat{\mathbf{C}}\| \Delta_1 + \delta_H). \end{aligned}$$

As for the norm of the matrix  $\widehat{\mathbf{C}}_{\text{loc}} \mathbf{C}_{\text{loc}}^{-1} - \widehat{\mathbf{C}} \mathbf{C}^{-1}$ , we use

$$\|\widehat{\mathbf{C}}_{\text{loc}} \mathbf{C}_{\text{loc}}^{-1} - \widehat{\mathbf{C}} \mathbf{C}^{-1}\| \leq \|(\mathbf{C}_{\text{loc}})^{-1} - \mathbf{C}^{-1}\| \|\widehat{\mathbf{C}}_{\text{loc}}\| + \|\widehat{\mathbf{C}}_{\text{loc}} - \widehat{\mathbf{C}}\| \|\mathbf{C}^{-1}\|.$$

From part (b), we have

$$\|\mathbf{C}_{\text{loc}}^{-1} - \mathbf{C}^{-1}\| \|\widehat{\mathbf{C}}_{\text{loc}}\| \leq \frac{\|\mathbf{C}^{-1}\|^2 \|\widehat{\mathbf{C}}\| \delta_C}{(1 - \delta_C \|\mathbf{C}^{-1}\|)(1 - \Delta_1 \|\widehat{\mathbf{C}}\|)}, \quad \|\widehat{\mathbf{C}}_{\text{loc}} - \widehat{\mathbf{C}}\| \|\mathbf{C}^{-1}\| \leq \frac{\|\mathbf{C}^{-1}\| \|\widehat{\mathbf{C}}\|^2 \Delta_1}{1 - \Delta_1 \|\widehat{\mathbf{C}}\|}.$$

In summary:

$$\begin{aligned} \|\hat{\mathbf{m}}_{\text{loc}} - \hat{\mathbf{m}}\| &\leq \left( \frac{\|\mathbf{C}^{-1}\|^2 \|\hat{\mathbf{C}}\| \delta_C}{(1 - \delta_C \|\mathbf{C}^{-1}\|)(1 - \Delta_1 \|\hat{\mathbf{C}}\|)} + \frac{\|\mathbf{C}^{-1}\| \|\hat{\mathbf{C}}\|^2 \Delta_1}{1 - \Delta_1 \|\hat{\mathbf{C}}\|} \right) \|\mathbf{m}\| \\ &\quad + \frac{\|\hat{\mathbf{C}}\| \|\mathbf{R}^{-1}\|}{1 - \Delta_1 \|\hat{\mathbf{C}}\|} (\|\hat{\mathbf{C}}\| \Delta_1 + \delta_H) \|\mathbf{y}\|. \end{aligned} \quad \blacksquare$$

**Proposition B.3.** *Let  $\mathbf{\Omega}$  be a prior precision matrix and  $\mathbf{H}$  be an observation matrix. Let  $\delta_\Omega$  and  $\delta_H$  be as defined in (3.10) and (3.4). Let  $\mathbf{\Omega}_{\text{loc}}$  and  $\mathbf{H}_{\text{loc}}$  be the localized precision and observation matrices, then*

- a) *If  $\delta_\Omega \leq \|\mathbf{\Omega}\|$ ,  $\Delta_2 \leq \|\hat{\mathbf{C}}\|^{-1}$ , the localization creates a small perturbation of the posterior precision and covariance matrix in the sense that  $\|\hat{\mathbf{C}}^{-1} - \hat{\mathbf{C}}_{\text{p,loc}}^{-1}\| \leq \Delta_2$  and*

$$\|\hat{\mathbf{C}} - \hat{\mathbf{C}}_{\text{p,loc}}\| \leq \frac{\|\hat{\mathbf{C}}\|^2 \Delta_2}{1 - \Delta_2 \|\hat{\mathbf{C}}\|}, \quad \text{where } \Delta_2 := \delta_\Omega + (2\delta_H + \delta_H^2) \|\mathbf{R}^{-1}\|.$$

- b) *Under the same conditions as in a), the localization creates a small perturbation of the posterior mean in the sense that*

$$\|\hat{\mathbf{m}}_{\text{p,loc}} - \hat{\mathbf{m}}\| \leq \frac{\|\hat{\mathbf{C}}\| \delta_\Omega + \|\mathbf{\Omega}\| \|\hat{\mathbf{C}}\|^2 \Delta_2}{1 - \Delta_2 \|\hat{\mathbf{C}}\|} \|\mathbf{m}\| + \frac{\|\hat{\mathbf{C}}\| \|\mathbf{R}^{-1}\|}{1 - \Delta_2 \|\hat{\mathbf{C}}\|} (\|\hat{\mathbf{C}}\| \Delta_2 + \delta_H) \|\mathbf{y}\|.$$

*Proof.* The proofs are very similar to the proofs of Proposition B.2. To prove a), we follow the proof of Proposition B.2 a) and find that  $\|\mathbf{\Omega} - \mathbf{\Omega}_{\text{loc}}\| \leq \delta_\Omega$ , and (B.1)

$$\|\mathbf{H}^T \mathbf{R}^{-1} \mathbf{H} - \mathbf{H}_{\text{loc}}^T \mathbf{R}^{-1} \mathbf{H}_{\text{loc}}\| \leq (2\delta_H + \delta_H^2) \|\mathbf{R}^{-1}\|.$$

Therefore

$$\|(\mathbf{\Omega} + \mathbf{H}^T \mathbf{R}^{-1} \mathbf{H}) - (\mathbf{\Omega}_{\text{loc}} + \mathbf{H}_{\text{loc}}^T \mathbf{R}^{-1} \mathbf{H}_{\text{loc}})\| \leq \delta_\Omega + (2\delta_H + \delta_H^2) \|\mathbf{R}^{-1}\| =: \Delta_2.$$

We apply Lemma B.1 to  $\hat{\mathbf{C}} = (\mathbf{\Omega} + \mathbf{H}^T \mathbf{R}^{-1} \mathbf{H})^{-1}$ ,

$$\|\hat{\mathbf{C}} - \hat{\mathbf{C}}_{\text{p,loc}}\| \leq \frac{\|\hat{\mathbf{C}}\|^2 \Delta_2}{1 - \Delta_2 \|\hat{\mathbf{C}}\|}.$$

As a consequence, we have that  $\|\hat{\mathbf{C}}_{\text{p,loc}}\| \leq \frac{\|\hat{\mathbf{C}}\|}{1 - \Delta_2 \|\hat{\mathbf{C}}\|}$ .

To prove claim b), we write

$$\hat{\mathbf{m}}_{\text{p,loc}} - \hat{\mathbf{m}} = (\hat{\mathbf{C}}_{\text{p,loc}} \mathbf{\Omega}_{\text{loc}} - \hat{\mathbf{C}} \mathbf{\Omega}) \mathbf{m} + (\hat{\mathbf{C}}_{\text{p,loc}} \mathbf{H}_{\text{loc}}^T - \hat{\mathbf{C}} \mathbf{H}^T) \mathbf{R}^{-1} \mathbf{y}.$$

The norm of the matrix  $(\hat{\mathbf{C}}_{\text{p,loc}} \mathbf{H}_{\text{loc}}^T - \hat{\mathbf{C}} \mathbf{H}^T) \mathbf{R}^{-1}$  can be bounded directly using claim a)

$$\begin{aligned} \|(\hat{\mathbf{C}}_{\text{p,loc}} \mathbf{H}_{\text{loc}}^T - \hat{\mathbf{C}} \mathbf{H}^T) \mathbf{R}^{-1}\| &\leq \|\hat{\mathbf{C}} - \hat{\mathbf{C}}_{\text{p,loc}}\| \|\mathbf{H}^T \mathbf{R}^{-1}\| + \|\hat{\mathbf{C}}_{\text{p,loc}}\| \|\mathbf{H}_{\text{loc}} - \mathbf{H}\| \|\mathbf{R}^{-1}\| \\ &\leq \frac{\|\hat{\mathbf{C}}\| \|\mathbf{R}^{-1}\|}{1 - \Delta_2 \|\hat{\mathbf{C}}\|} (\|\hat{\mathbf{C}}\| \Delta_2 + \delta_H). \end{aligned}$$

The norm of the matrix  $\widehat{\mathbf{C}}_{p,\text{loc}}\boldsymbol{\Omega}_{\text{loc}} - \widehat{\mathbf{C}}\boldsymbol{\Omega}$  can be bounded by

$$\|\widehat{\mathbf{C}}_{p,\text{loc}}\boldsymbol{\Omega}_{\text{loc}} - \widehat{\mathbf{C}}\boldsymbol{\Omega}\| \leq \|\boldsymbol{\Omega}_{\text{loc}} - \boldsymbol{\Omega}\| \|\widehat{\mathbf{C}}_{p,\text{loc}}\| + \|\widehat{\mathbf{C}}_{p,\text{loc}} - \widehat{\mathbf{C}}\| \|\boldsymbol{\Omega}\|.$$

From part (a), we have

$$\|\boldsymbol{\Omega}_{\text{loc}} - \boldsymbol{\Omega}\| \|\widehat{\mathbf{C}}_{p,\text{loc}}\| \leq \frac{\|\widehat{\mathbf{C}}\| \delta_{\Omega}}{1 - \Delta_2 \|\widehat{\mathbf{C}}\|}, \quad \|\widehat{\mathbf{C}}_{p,\text{loc}} - \widehat{\mathbf{C}}\| \|\boldsymbol{\Omega}\| \leq \frac{\|\boldsymbol{\Omega}\| \|\widehat{\mathbf{C}}\|^2 \Delta_2}{1 - \Delta_2 \|\widehat{\mathbf{C}}\|}.$$

In summary:

$$\|\widehat{\mathbf{m}}_{p,\text{loc}} - \widehat{\mathbf{m}}\| \leq \frac{\|\widehat{\mathbf{C}}\| \delta_{\Omega} + \|\boldsymbol{\Omega}\| \|\widehat{\mathbf{C}}\|^2 \Delta_2}{1 - \Delta_2 \|\widehat{\mathbf{C}}\|} \|\mathbf{m}\| + \frac{\|\widehat{\mathbf{C}}\| \|\mathbf{R}^{-1}\|}{1 - \Delta_2 \|\widehat{\mathbf{C}}\|} (\|\widehat{\mathbf{C}}\| \Delta_2 + \delta_H) \|\mathbf{y}\|. \quad \blacksquare$$

## REFERENCES

- [1] S. AGAPIOU, O. PAPASPILOPOULOS, D. SANZ-ALONSO, AND A. STUART, *Importance sampling: computational complexity and intrinsic dimension*, Stat. Sci., 32 (2017), pp. 405–431.
- [2] A. BESKOS, A. JASRA, E. MUZAFFER, AND A. STUART, *Sequential Monte Carlo methods for Bayesian elliptic inverse problems*, Stat. Comp., 25 (2015), pp. 727–737.
- [3] A. BESKOS, N. PILLAI, G. ROBERTS, J.-M. SANZ-SERNA, AND A. STUART, *Optimal tuning of the hybrid Monte Carlo algorithm*, Bernoulli, 19 (2013), pp. 1501–1534.
- [4] A. BESKOS, G. ROBERTS, AND A. STUART, *Optimal scalings for local Metropolis-Hastings chains on nonproduct targets in high dimensions*, Ann. Appl. Probab., 19 (2009), pp. 863–898.
- [5] P. BICKEL AND E. LEVINA, *Regularized estimation of large covariance matrices*, Ann. Statist., 36 (2008), pp. 199–227.
- [6] P. BICKEL AND M. LINDNER, *Approximating the inverse of banded matrices by banded matrices with applications to probability and statistics*, Theory Probab. Appl., 56 (2012), pp. 1–20.
- [7] P. J. BICKEL AND E. LEVINA, *Regularized estimation of large covariance matrices*, Ann. Stat., 36 (2008), pp. 199–227.
- [8] T. BUI-THANH, O. GHATTAS, J. MARTIN, AND G. STADLER, *A computational framework for infinite-dimensional Bayesian inverse problems. Part I: The linearized case, with application to global seismic inversion*, SIAM J. Sci. Comput., 36 (2013), pp. A2494–A2523.
- [9] A. CHORIN AND M. MORZFELD, *Conditions for successful data assimilation*, J. Geophys. Res., 118 (2013), pp. 11,522–11,533.
- [10] O. F. CHRISTENSEN, G. O. ROBERTS, AND J. S. ROSENTHAL, *Scaling limits for the transient phase of local Metropolis–Hastings algorithms*, Journal of the Royal Statistical Society: Series B (Statistical Methodology), 67 (2005), pp. 253–268.
- [11] S. COTTER, G. ROBERTS, A. STUART, AND D. WHITE, *MCMC methods for functions: modifying old algorithms to make them faster*, Stat. Sci., 28 (2013), pp. 424–446.
- [12] T. CUI, K. J. H. LAW, AND Y. M. MARZOUK, *Dimension-independent likelihood-informed MCMC*, J. Comput. Phys., 304 (2016), pp. 109–137.
- [13] T. CUI, J. MARTIN, Y. M. MARZOUK, A. SOLONEN, AND A. SPANTINI, *Likelihood-informed dimension reduction for nonlinear inverse problems*, Inverse Probl., 29 (2014), p. 114015.
- [14] T. CUI, Y. M. MARZOUK, AND K. WILLCOX, *Scalable posterior approximations for large-scale Bayesian inverse problems via likelihood-informed parameter and state reduction*, J. Comput. Phys., 315 (2016), pp. 363–387.
- [15] S. DUANE, A. KENNEDY, B. PENDLETON, AND D. ROWETH, *Hybrid Monte Carlo*, Phys. Lett. B, 195 (1987), pp. 216–222.
- [16] G. EVENSEN, *Data assimilation: the ensemble Kalman filter*, Springer, 2006.

- [17] H. FLATH, L. WILCOX, V. AKÇELİK, J. HILL, B. VAN BLOEMEN WAANDER, AND O. GHATTAS, *Fast algorithms for Bayesian uncertainty quantification in large-scale linear inverse problems based on low-rank partial Hessian approximations*, SIAM J. Sci. Comput., 33 (2011), pp. 407–432.
- [18] D. FOREMAN-MACKEY, A. CONLEY, W. MEIERJURGEN FARR, D. W. HOGG, D. LONG, P. MARSHALL, A. PRICE-WHELAN, J. SANDERS, AND J. ZUNTZ, *emcee: The MCMC Hammer*. Astrophysics Source Code Library, Mar. 2013, <https://arxiv.org/abs/1303.002>.
- [19] A. GALLI AND G. H., *Rate of convergence of the Gibbs sampler in the Gaussian case*, Math. Geol., 33 (2001), pp. 653–677.
- [20] G. GASPARI AND S. COHN, *Construction of correlation functions in two and three dimensions*, Q. J. R. Meteorol. Soc., 125 (1999), pp. 723–757.
- [21] J. GOODMAN AND A. D. SOCKAL, *Multigrid Monte Carlo method. conceptual foundation*, Phys. Rev. D, 40 (1989), pp. 2035–2071.
- [22] J. GOODMAN AND J. WEARE, *Ensemble samplers with affine invariance*, Comm. App. Math. Com. Sc., 5 (2010), pp. 65–80.
- [23] M. HAIRER, A. M. STUART, AND S. J. VOLLMER, *Spectral gaps for a Metropolis–Hastings algorithm in infinite dimensions*, The Annals of Applied Probability, 24 (2014), pp. 2455–2490.
- [24] T. M. HAMILL, J. WHITAKER, AND C. SNYDER, *Distance-dependent filtering of background covariance estimates in an ensemble Kalman filter*, Mon. Weather Rev., 129 (2001), pp. 2776–2790.
- [25] P. HOUTEKAMER AND H. MITCHELL, *A sequential ensemble Kalman filter for atmospheric data assimilation*, Mon. Weather Rev., 129 (2001), pp. 123–136.
- [26] P. L. HOUTEKAMER, H. L. MITCHELL, G. PELLERIN, M. BUEHNER, M. CHARRON, L. SPACEK, AND B. HANSEN, *Atmospheric data assimilation with an ensemble Kalman filter: Results with real observations*, Mon. Weather Rev., 133 (2005), pp. 604–620.
- [27] M. KALOS AND P. WHITLOCK, *Monte Carlo methods*, vol. 1, John Wiley & Sons, 1 ed., 1986.
- [28] Y. LEE AND A. MAJDA, *State estimation and prediction using clustered particle filters*, Proc. Natl. Acad. Sci. U.S.A. Proc. Natl. Acad. Sci. U.S.A., 113 (2016), pp. 14609–14614.
- [29] J. LEI AND P. BICKEL, *A moment matching ensemble filter for nonlinear non-Gaussian data assimilation*, Mon. Weather Rev., 139 (2011), pp. 3964 – 3973.
- [30] F. LINDGREN, H. RUE, AND J. LINDSTRÖM, *An explicit link between Gaussian fields and Gaussian Markov random fields: the stochastic partial differential equation approach*, Journal of the Royal Statistical Society: Series B (Statistical Methodology), 73 (2011), pp. 423–498.
- [31] D. MACKAY, *Introduction to Monte Carlo methods*, in Learning in Graphical Models, M. I. Jordan, ed., NATO Science Series, Kluwer Academic Press, 1998, pp. 175–204.
- [32] A. J. MAJDA AND X. T. TONG, *Performance of ensemble Kalman filters in large dimensions*. Accepted by Comm. Pure Appl. Math. arXiv: 1606.09321, 2017.
- [33] J. MARTIN, L. C. WILCOX, C. BURSTEDDE, AND O. GHATTAS, *A stochastic Newton MCMC method for large-scale statistical inverse problems with application to seismic inversion*, SIAM J. Sci. Comput., 34 (2012), pp. A1460–A1487.
- [34] M. MORZFELD, D. HODYSS, AND C. SNYDER, *What the collapse of the ensemble Kalman filter tells us about particle filters*, Tellus A, 69 (2017), p. 1283809.
- [35] R. NEAL, *MCMC using Hamiltonian dynamics*, in Handbook of Markov Chain Monte Carlo, S. Brooks, A. Gelman, G. Jones, and X.-L. Meng, eds., Chapman & Hall, Oxford, 2011, ch. 5.
- [36] A. OWEN, *Monte Carlo Theory, Methods and Examples*, 2013.
- [37] S. PENNY AND T. MIYOSHI, *A local particle filter for high dimensional geophysical systems*, Nonlinear Process Geophys., 2 (2015), pp. 1631–1658.
- [38] N. PETRA, J. MARTIN, G. STADLER, AND O. GHATTAS, *A computational framework for infinite-dimensional Bayesian inverse problems. Part II: Stochastic Newton MCMC with application to ice sheet flow inverse problems*, SIAM J. Sci. Comput., 36 (2013), pp. A1525–1555.
- [39] J. POTERJOY, *A localized particle filter for high-dimensional nonlinear systems*, Mon. Weather Rev., 144 (2015), pp. 59 – 76.
- [40] J. POTERJOY AND J. ANDERSON, *Efficient assimilation of simulated observations in a high-dimensional geophysical system using a localized particle filter*, Mon. Weather Rev., 144 (2016), pp. 2007–2020.
- [41] J. POTERJOY, R. SOBASH, AND J. ANDERSON, *Convective-scale data assimilation for the weather research and forecasting model using the local particle filter*, Mon. Weather Rev., 145 (2017), pp. 1897–1918.



- [42] P. REBESCHINI AND R. VAN HANDEL, *Can local particle filters beat the curse of dimensionality?*, Ann. Appl. Probab., 25 (2015), pp. 2809 – 2866.
- [43] S. REICH, *A nonparametric ensemble transform method for Bayesian inference*, Mon. Weather Rev., 35 (2013), pp. 1337–1367.
- [44] G. ROBERTS, A. GELMAN, AND W. GILKS, *Weak convergence and optimal scaling of random walk Metropolis algorithms*, Ann. Appl. Probab., 7 (1997), pp. 110–120.
- [45] G. ROBERTS AND J. ROSENTHAL, *Optimal scaling of discrete approximations to Langevin diffusions*, J. R. Stat. Soc. Ser: B Stat. Methodol., 60 (1998), pp. 255–268.
- [46] G. O. ROBERTS AND S. S. K., *Updating schemes, correlation structure, blocking and parameterization for the Gibbs sampler*, J. R. Stat. Soc. Ser: B Stat. Methodol., 59 (1997), pp. 291–317.
- [47] H. RUE AND L. HELD, *Gaussian Markov random fields: theory and applications*, CRC press, 2005.
- [48] A. SPANTINI, D. BIGONI, AND Y. M. MARZOUK, *Inference via low-dimensional couplings*. arXiv:1703.06131, 2017.
- [49] A. SPANTINI, A. SOLONEN, T. CUI, J. MARTIN, L. TENORIO, AND Y. M. MARZOUK, *Optimal low-rank approximations of Bayesian linear inverse problems*, SIAM J. Sci. Comput., 37 (2015), pp. A2451–A2487.
- [50] A. STUART, *Inverse problems: a Bayesian perspective*, Acta Numer., 19 (2010), pp. 451–559.
- [51] M. TIPPET, J. ANDERSON, C. BISHOP, T. HAMILL, AND J. WHITAKER, *Ensemble square root filters*, Mon. Weather Rev., 131 (2003), pp. 1485–1490.
- [52] J. TÖDTER AND B. AHRENS, *A second-order exact ensemble square root filter for nonlinear data assimilation*, Mon. Weather Rev., 143 (2015), pp. 1337–1367.
- [53] X. T. TONG, *Performance analysis of local ensemble Kalman filter*. arXiv:1705.10598.
- [54] P. VAN LEEUWEN, Y. CHENG, AND S. REICH, *Nonlinear Data Assimilation*, Springer, 2015.
- [55] U. WOLFF, *Monte Carlo errors with less errors*, Comput. Phys. Commun., 156 (2004), pp. 143–153.